SCIEPublish

Article

Modular Transcriptional Regulation Using Switchable Transcription Terminators and Aptamers: Design and Optimization in Synthetic Biology

Jiayan Jiao [1], Minghong Shi [1], Shuting Zheng [1], Xianai Shi [1,2,*] and Shaobin Guo [1,2,*]

[1] College of Biological Science and Engineering, Fuzhou University, Fuzhou 350108, China; JJYJSWTXQ591144528@163.com (J.J.); shiminghong2022@163.com (M.S.); Zhengst09@163.com (S.Z.)

[2] Fujian Key Laboratory of Medical Instrument and Pharmaceutical Technology, Fuzhou University, Fuzhou 350108, China

* Corresponding authors. E-mail: shixa@fzu.edu.cn (X.S.), sguo@fzu.edu.cn (S.G.)

Received: 7 April 2025; Accepted: 27 May 2025; Available online: 4 June 2025

ABSTRACT: Transcriptional regulation is a key step in gene expression control. While transcription factor-based regulation has been widely used and offers robust control over gene expression, it can sometimes face challenges such as achieving high specificity, rapid dynamic responses, and fine-tuned regulatory precision, which have motivated the exploration of alternative regulatory strategies. With the development of synthetic biology, novel genetic elements such as Switchable Transcription Terminators (SWT) and aptamers provide more flexible and programmable strategies for transcriptional regulation. However, the independent regulatory capabilities of these two types of elements and their combined regulatory mechanisms still require further investigation. In this study, based on an *in vitro* transcription system, we systematically explored the transcriptional regulation potential of SWT and aptamers. We innovatively combined these two elements to construct a modular gene expression regulation system. First, we screened and optimized a series of SWTs, obtaining high-performance SWTs with low leakage expression and high ON/OFF ratios. These were further validated for reproducibility of their regulatory performance in *E. coli*. Next, we constructed multi-level cascading circuits using SWTs, successfully extending the system to six levels and building four types of biological logic gates based on SWT *in vitro*: AND gate, NOT gate, NAND gate, and NOR gate. Furthermore, based on a previously identified thrombin aptamer capable of transcriptional regulation, we confirmed that ligand binding significantly promoted gene transcription. Finally, we integrate switchable transcription terminators (SWTs) and aptamers to create a modular, ligand-responsive system. We combined aptamers with SWTs to construct heterologous input logic gates, successfully improving the precision and dynamic range of regulation. Compared to the individual regulation of SWT and aptamer, the Aptamer-SWT synergistic regulation enhanced transcription activation by up to 3.3-fold and 7.84-fold, respectively. Additionally, we co-utilized these two genetic elements to construct heterologous input AND and OR gates *in vitro*. This study expands the strategies for gene expression regulation and provides new elements and theoretical support for efficient, programmable transcriptional regulation in synthetic biology. This system holds potential for biosensing, gene circuit design, and nucleic acid therapy applications.

Keywords: Synthetic biology; Transcriptional regulation; Switchable transcription terminators; Aptamers; Biological logic gates; Cascading reaction

1. Introduction

Gene expression regulation is one of the core research directions in synthetic biology. Transcriptional regulation, as the first checkpoint of gene expression, directly affects cells' physiological state and functional capabilities, such as cell development and differentiation, stress responses, tissue homeostasis, and immunity [1]. Traditional transcriptional regulation methods primarily rely on transcription factors and cis/trans-acting elements; however, these methods suffer from low specificity [2,3], high regulatory complexity [4], and limited programmability, making it difficult to meet the needs of complex gene circuit designs. In recent years, with the development of novel RNA regulatory elements and strategies, such as the CRISPR/Cas systems [5], riboregulators [6], aptamers [7], and switchable transcription terminators (SWTs) [8,9], synthetic biology has made significant progress in flexible, efficient, and programmable

https://doi.org/10.70322/sbe.2025.10009

transcriptional regulation. For example, Chappell et al. constructed synthetic small transcription-activating RNAs (STARs) and successfully created RNA-based transcriptional regulatory logic gates, expanding the capacity of sRNA to regulate gene expression [10]. Manja et al. used theophylline aptamer-based sensing units to construct a new type of riboregulator, which was verified in *E. coli* to regulate not only translation but also transcription [11].

Riboregulators are RNA elements capable of regulating gene expression. Compared to traditional regulatory methods, these novel genetic elements offer advantages such as strong programmability, rapid response, and good biocompatibility [12,13]. Riboregulators respond to a variety of signals, including DNA, RNA, large molecules like proteins, small molecules, and even environmental factors [14–17]. The diversity of trigger signals enhances the adaptability, flexibility, and dynamics of these regulatory elements while also improving the robustness of biological systems. This has led to the widespread application of DNA or RNA regulatory elements in metabolic pathway engineering [18], synthetic gene circuit construction [19], biosensor development [20,21], and the development of synthetic regulators for induced gene expression [22,23]. Among them, the toehold switch is a classic type of riboregulator. As an RNA element capable of regulating transcription, it can respond to arbitrary complementary RNAs by initiating RNA-RNA strand displacement through toehold-mediated linear interactions. In addition, through rational design, the toehold switch can conceal or expose the ribosome binding site (RBS), thereby also enabling control over translation initiation [16]. Although significant progress has been made in studying the role of riboregulators in gene expression control, research and application for precise transcriptional regulation remain limited. To achieve precise control of the transcription process, inspired by the design of STARs, Hong et al. developed a gene switch known as the Switchable Transcription Terminator (SWT), which controls both transcription and translation processes in *E. coli*. They also constructed an AND gate at the translation level [8]. Subsequently, we systematically explored the design strategies for switchable transcription terminators and, by optimizing the structure, created high-performance SWTs, which displayed a 283-fold activation change when triggered by an input homologous RNA trigger. Additionally, we developed and optimized an automatic design algorithm that can output random SWT sequences, enhancing the programmability and flexibility of SWT design. We also successfully constructed a three-layer cascading circuit and a dual-input three-layer OR gate *in vitro*, laying the foundation for more complex logic operations using gene circuits [9]. The optimized SWT structure is divided into four regions: Toehold Regionregion, Stem Regionregion, Loop Regionregion, and U tract, with the Stem Regionregion, Loop Regionregion, and U tract forming the Terminator Regionregion (Figure 1A).

The entire Terminator region can be replaced with other natural or synthetic terminator sequences. In this study, we selected the synthetic terminator T500, which has a termination efficiency of 98%, as the SWT structural component [24,25]. We also attached an optimized Broccoli fluorescent aptamer 3WJdB [26] after the switchable transcription terminator as a reporter gene to characterize the transcription results. 3WJdB (Three-Way Junction Broccoli) is an RNA structure engineered from the Broccoli RNA fluorescent aptamer. The dimeric Broccoli (dB) aptamer is assembled into a single unit via a three-way junction (3WJ) structure derived from the packaging RNA of bacteriophage Φ29 [27–29]. Compared to the unmodified Broccoli aptamer, this redesigned and optimized version exhibits improved structural stability and enhanced fluorescence signal upon binding with a fluorescent dye. The optimized aptamer specifically binds to the dye DFHBI-1T (purchased from Sigma-Aldrich, St. Louis, MO, USA, catalog number SML2697) and generates a strong fluorescence signal (excitation/emission = 472 nm/507 nm) [30]. It has been widely applied in characterizing gene circuit outputs [31,32], monitoring transcriptional activity [33,34], and in cell-free systems [35]. The mechanism of SWT functions by binding to a SWT trigger that is complementary to both the Toehold region and the Stem region, thereby enabling the transition from the transcription OFF state to the ON state (Figure 1B).

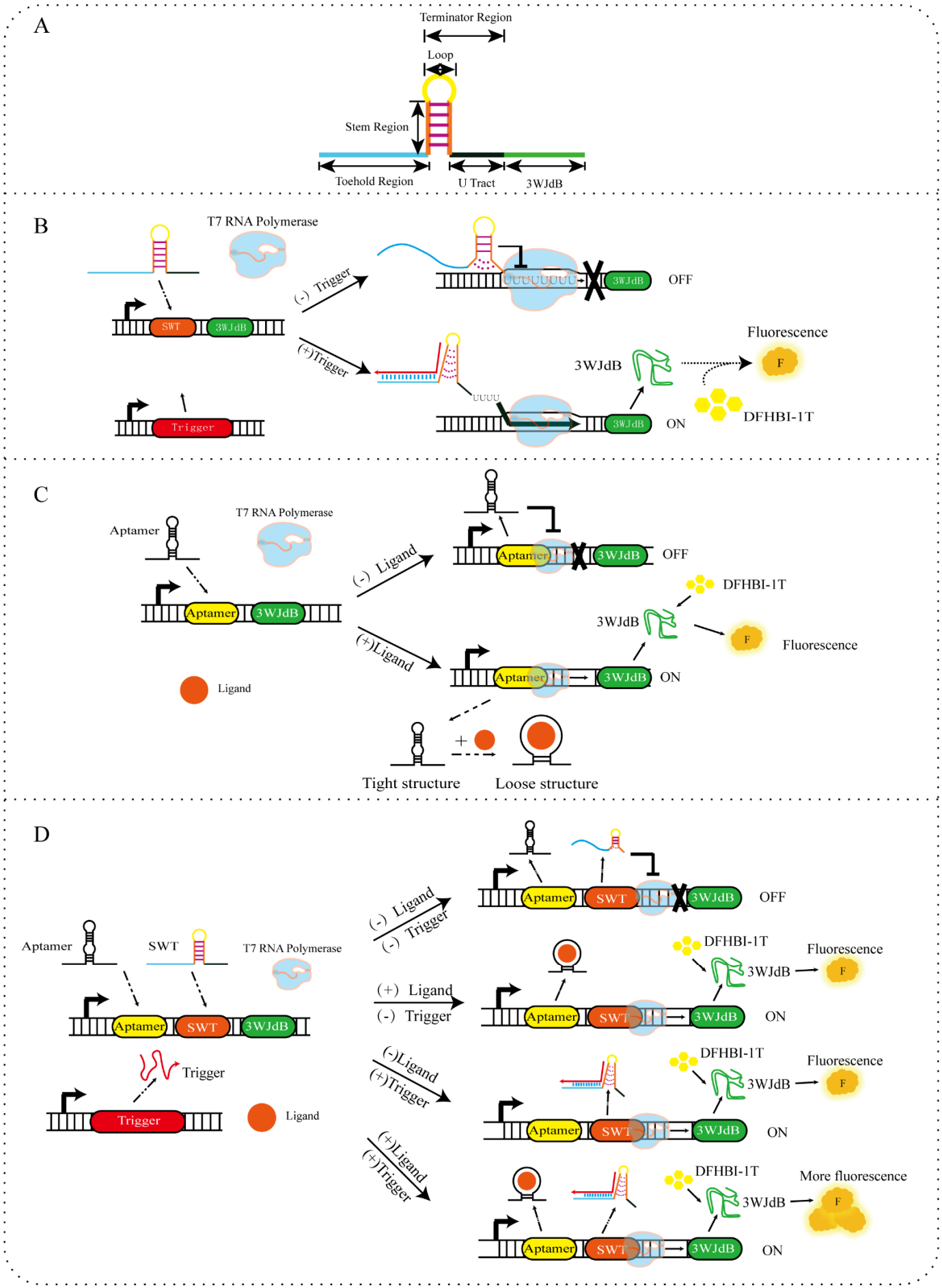

Figure 1. (**A**) SWT structure: The entire SWT consists of the Toehold region, Stem region, Loop region, and U tract, followed by a reporter gene 3WJdB to characterize the transcription results. The Toehold region provides a binding platform for RNA

polymerase (RNAP) and helps stabilize the overall structure to some extent. The Stem region is a reverse complementary sequence that links the Toehold region, Loop region, and U tract, providing mechanical support to the hairpin structure, ensuring its stable formation, and preventing RNAP from continuing elongation. The Loop region, located at the top of the hairpin structure, is the key area recognized by RNAP, triggering RNAP pausing and promoting transcription termination. The U tract, located at the tail of the hairpin structure, consists of a continuous uracil (U) nucleotide sequence and is crucial for RNAP's release of the template. It works in synergy with the hairpin structure to induce RNA chain dissociation. (**B**) Mechanism of SWT: In the absence of a SWT trigger, the hairpin structure of the SWT itself obstructs T7 RNA polymerase (T7 RNAP) from extending downstream, preventing transcription from proceeding normally (OFF). When a trigger is present, it binds complementarily to part of the SWT structure, disrupting the hairpin structure, allowing T7 RNAP to continue elongating downstream, and enabling normal transcription to occur (ON). (**C**) Construction and mechanism of aptamer switch: By embedding the aptamer between the promoter and the reporter gene 3WJdB, an aptamer switch is constructed. In the absence of ligand input, the secondary structure of the aptamer itself hinders T7 RNA polymerase elongation (OFF). Upon ligand binding, the aptamer undergoes conformational changes, which may loosen the surrounding structure, thereby facilitating the downstream gene transcription (ON). (**D**) Construction of a transcriptional regulation switch by Integrating aptamer and SWT: By combining SWT with the aptamer, the integration of these two distinct mechanisms may further enhance transcriptional efficiency. In the absence of any input, the aptamer and SWT form a complex secondary structure that hinders the elongation of T7 RNA polymerase (OFF). Upon ligand input, the conformational changes induced by aptamer-ligand binding may disrupt the SWT structure, making it more relaxed and thereby facilitating transcription (ON). When the SWT trigger is introduced, the disruption of the SWT structure significantly enhances transcription (ON). Furthermore, when both the ligand and the SWT trigger are simultaneously introduced, the two elements work synergistically to promote transcription further, resulting in a stronger fluorescence signal output (ON).

In order to respond to more complex environmental signals and integrate sensing with regulation, it is necessary to explore more flexible biological elements. Aptamers, due to their high specificity and affinity for target ligand molecules, and the conformational changes induced upon ligand binding, can disrupt gene expression, making them potential regulatory biological elements for gene expression. Aptamers are single-stranded DNA or RNA sequences that are selected through SELEX (Systematic Evolution of Ligands by Exponential Enrichment) technology and can bind small molecules [36,37], biomacromolecules [38,39], cells [40–42], and other targets [43,44]. With the advancement of synthetic biology, SELEX technology has continuously been innovated. We developed a new aptamer selection technique called CIVT-SELEX, which combines Capture-SELEX and *in vitro* transcription (IVT) systems to screen aptamers suitable for transcriptional regulation. We successfully identified a single-stranded DNA aptamer with specificity for thrombin and validated its potential for transcriptional regulation of downstream genes. This demonstrated the feasibility and robustness of the aptamer as a genetic element in linear DNA and plasmids, expanding the transcriptional regulation toolkit [45]. While previous research on aptamers focused on areas such as biosensing, detection, nanostructures, and drug delivery, significant progress has also been made in applying aptamers to gene regulation. For instance, Heonjoon et al. developed a method called ARTIST based on strand displacement reactions and uses DNA templates for aptamer-regulated transcription (dARTs) to construct protein biosensors that can detect multiple targets quickly. This method also integrates easily with downstream circuits to output different types of signals [46]. Although aptamers have been applied to gene expression regulation, current aptamer-based regulatory strategies still face issues such as significant leakage expression, insufficient regulatory precision, and limited dynamic range.

Therefore, we aimed to explore the transcriptional regulatory potential of two genetic elements, SWT and aptamer, based on an *in vitro* transcription system and innovatively combined these two genetic elements to regulate transcription. On the one hand, we also designed the aptamer in the form of a genetic switch to further explore its potential in transcriptional regulation. The conformational changes induced by aptamer-ligand binding may loosen the surrounding structure, thereby facilitating transcription (Figure 1C). On the other hand, the integration of SWTs with aptamer-based regulation leverages the strengths of both systems to achieve precise, ligand-responsive transcriptional control. SWTs provide a robust mechanism for transcription termination, but their regulation is often limited to sequence-intrinsic properties. On the other hand, aptamers offer high specificity for ligand binding, allowing external signals to modulate gene expression. By embedding aptamers within or adjacent to the SWT structure, ligand binding can induce conformational changes that alter the efficiency of transcription termination. This combination enables dynamic, tunable control over gene expression in response to specific molecular cues, making it particularly valuable for synthetic biology applications where modular and programmable regulation is essential (Figure 1D). To our knowledge, no prior studies have merged SWTs with aptamers for synergistic transcriptional control.

In this work, we screened and optimized a series of SWTs to improve their ON/OFF ratio and orthogonality and constructed six-layer cascaded circuits as well as multiple biological logic gates. Additionally, we validated that thrombin aptamers, upon ligand binding, can promote transcription to some extent. Furthermore, by combining

Aptamers with SWTs, we successfully enhanced the precision and dynamic range of transcriptional regulation, expanding new strategies for gene expression regulation. Our study provides new tools and theoretical support for gene circuit optimization, biosensor development, and precise nucleic acid regulation in the field of synthetic biology.

2. Materials and Methods

They should be described with sufficient detail to allow others to replicate and build on published results. New methods and protocols should be described in detail, while well-established methods can be briefly described and appropriately cited. Give the name and version of any software used and clarify whether the computer code is available. Include any pre-registration codes.

2.1. Materials

2.1.1. Plasmid

pSG81 (Ampicillin resistance, used for constructing recombinant plasmids related to *in vitro* transcription studies, from Our lab, addgene ID is #102454, https://www.addgene.org/search/catalog/plasmids/?q=PSG81 (accessed on 1 September 2023), the plasmid map is shown in Figure S1). pQT30-T7 RNAPol (Chloramphenicol resistance, used for expressing T7 RNA polymerase, from Tianjin Institute of Life Sciences, Tianjin, China). pUC57 (Ampicillin resistance, used to verify the transcriptional regulation performance of SWT in *E. coli*, from Jiangsu Saisofei Biotechnology Co., Ltd., Nantong, China). pSG22 (Kanamycin resistance, used to verify the transcriptional regulation performance of SWT in *E. coli*, from Our lab, addgene ID is #102451, https://www.addgene.org/search/catalog/plasmids/?q=pSG22 (accessed on 1 September 2023), the plasmid map is shown in Figure S2).

2.1.2. Strains

E. coli TOP10 Chemically Competent Cell (ZC104), genotype is F- mcrAΔ(mrr-hsdRMS-mcrBC) φ80 lacZΔM15 ΔlacX74 recA1 araΔ139Δ(ara-leu)7697 galU galK rps L(strr)endA1 nupG, used for efficient DNA cloning and plasmid amplification (Beijing Zomanbio, Beijing, China). *E. coli* DH5α Chemically Competent Cell (ZC101), genotype is F- φ80 lacZΔM15Δ (lacZYA-argF) U169 endA1 recA1 hsdR17(rK−,mK+) sup E44 λ- thi-1 gyrA96 relA1 phoA, facilitates stable DNA cloning and high-purity plasmid DNA extraction (Beijing Zomanbio). *E. coli* BL21(DE3) Chemically Competent Cell (ZC121), genotype is F- ompT hsdS(rB-mB-) gal dcm (DE3), used for high-level expression of non-toxic proteins (Beijing Zomanbio).

2.2. Methods

2.2.1. Preparation of Linear DNA for *In Vitro* Transcription

In this study, all the DNA templates used for *in vitro* transcription assays were prepared as linearized DNA fragments. First, recombinant plasmids were constructed using two seamless cloning methods: Golden Gate Assembly (GGA) or Gibson Assembly. A 5 μL aliquot of the ligation product was chemically transformed into 50 μL of *E. coli* Top10 or DH5α competent cells. The transformed cells were plated on LB agar containing the appropriate antibiotic and incubated at 37 °C in an inverted position for 12–16 h. Then pick the single colonies for colony PCR (cPCR) and sequencing verification. Correct constructs were subjected to plasmid miniprep using the plasmid extraction kit (Nanjing Novozan, Nanjing, China). The linear DNA fragments for *in vitro* transcription were then amplified via PCR, followed by Dpn I digestion to eliminate the template plasmid. Agarose gel electrophoresis was performed to verify the integrity of the PCR products, which were subsequently purified using the DNA Purification Kit (Nanjing Novozan). Finally, the concentration of the linear DNA was adjusted to 30 ng/μL.

2.2.2. Secondary Structure Prediction of SWT and Aptamer

The secondary structure of the candidate SWTs and aptamers was predicted using NUPACK [47] (Parameters: rna06; Ensemble: All stacking; Salts: Na^+ 1.0 M, Mg^{2+} 0.0 M; Concentrations: 10 nM; Temperature: 37 ℃; Max complex size: 2) and the Mfold (Sequence: linear; Temperature: 37 ℃; Ionic conditions: 1 M NaCl, no divalent ions) online tool.

2.2.3. The Prediction and Characterization of Aptamer-Ligand Interactions

The three-dimensional conformation of aptamer-ligand interactions was predicted through simulation on the AlphaFold 3 [48] (Copies: 1) online platform. The aptamers with higher scores were further subjected to molecular docking and visualization using PyMOL.

2.2.4. Aptamer Circular Dichroism (CD) Characterization

The single-stranded DNA (ssDNA) aptamers (TBA15, TBA29, TBA61) were directly synthesized. The preparation method for single-stranded RNA (ssRNA) aptamer (TBA25) is as follows: a single-stranded DNA with a T7 promoter and the target gene was synthesized, then annealed to form double-stranded DNA (the annealing program was: 95 °C for 10 min for high-temperature denaturation, followed by −0.5 °C/8 s for each cycle, continuing for 140 cycles, until the temperature dropped to 25 °C and held for 5 min, then stored at 4 °C). This double-stranded DNA was transcribed in a cell-free transcription system for 8 h. After transcription, DNase I was used to digest any untranscribed DNA templates for 2 h. The resulting RNA was then purified using an RNA purification kit (Sangon Biotech, Shanghai, China) and stored at −20 °C. Before testing, 1 × Binding Buffer was prepared, containing 500 nM of the ligand Thrombin (Sigma-Aldrich, St. Louis, MO, USA), 5 μM of the nucleic acid aptamers (ssDNA, ssRNA), and mixtures of aptamers and ligands at the same concentrations (the total volume for each sample was 200 μL). The ssDNA and ssRNA groups were incubated at 95 °C for 10 min and immediately placed on ice to reduce the formation of their secondary structures before adding the ligand. After 1 h of incubation with the target ligand, the samples were subjected to CD spectroscopy analysis. To accurately characterize the changes induced by aptamer-ligand binding, the ligand-only curve was used as a baseline for zeroing. The parameters for the actual test were: nitrogen flow rate 4–5 L/min, scanning wavelength from 200 nm to 320 nm, scanning speed 50 nm/min, bandwidth 1 nm, and data averaging from 3 accumulated scans.

2.2.5. *In Vitro* Transcription Fluorescence Signal Measurement and Analysis

For the *in vitro* transcription system, the following components were mixed to a final volume of 10 μL: DNA template (concentration based on experimental needs), 10 × Buffer (400 mM Tris, 60 mM $MgCl_2$, 20 mM spermidine, 10 mM DTT, and adjust the pH to 7.9 with HCl) 1 μL, rNTPs (0.5 mM) 0.8 μL, T7 RNA polymerase (50 U) 0.9 μL, RNase inhibitor (10 U) 0.25 μL, DFHBI-1T (40 μM) 0.84 μL, DEPC-treated water to adjust the volume to 10 μL. The transcription reaction was prepared in triplicate. After preparation, the mixture was thoroughly vortexed, centrifuged, and transferred to a 384-well plate. The plate was then placed in a microplate reader for detection under the following conditions: temperature is 37 °C, incubation time is 2 h, the excitation wavelength is 472 nm, the emission wavelength is 507 nm, and the detection mode is reading from the bottom. For the analysis of the *in vitro* transcription results, the following calculation method is used:

$$\text{Normalized Fluorescence} = \text{Fluorescence} - \text{Background} \quad (1)$$

$$\text{Fold Change} = (\text{Normalized Fluorescence}_{ON}) \,/\, (\text{Normalized Fluorescence}_{OFF}) \quad (2)$$

2.2.6. *In Vivo* Fluorescence Signal Measurement and Analysis in *E. coli*

5 SWTs recombinant plasmids (ZS1, JS2, ZS16, ZS19, and ZS22), which exhibited good performance in *in vitro* tests, were constructed and introduced into *E. coli* BL21(DE3) competent cells. After verification by colony PCR (cPCR) and sequencing, 2 mL of LB liquid medium (with antibiotics added at 1/1000 of the medium volume) was inoculated and grown until the optical density (OD) reached 0.2–0.4. Then, 2 μL of IPTG (1 M) was added to achieve a final concentration of 1 mM. The cells were cultured at 25 °C with shaking at 200 rpm for 8–12 h to induce the expression of T7 RNA polymerase (T7 RNAP) in *E. coli* BL21 (DE3). After induction, 1 mL of bacterial culture was centrifuged at 5000 rpm for 1 min, and the supernatant was discarded. The bacterial pellet was resuspended in 1 mL of PBS buffer, and 100 μL of this suspension was mixed with 0.8 μL of DFHBI-1T (25 mM) to a final concentration of 200 μM. The mixture was incubated at 37 °C, 220 rpm, in the dark for 1 h. Fluorescence signals were measured using a fluorescence reader. The *in vivo* fluorescence measurement results were analyzed using the following formula:

$$\text{Normalized Fluorescence} = \text{Fluorescence/OD} - \text{Background/OD} \quad (3)$$

3. Results

3.1. Characterization of SWT Performance

SWT (switchable transcription terminator) is a type of transcriptional regulatory element based on the dynamic structural changes of RNA. Its core principle relies on the variability of RNA secondary structures, enabling controlled transcription termination or resumption in response to specific input signals (e.g., trigger RNA). Previous studies have optimized the structure and algorithm of SWT. To further investigate the transcriptional regulation efficiency of SWT and achieve precise control over the transcription process, we need to validate the SWT sequences generated by the algorithm. An ideal SWT should exhibit low leakage, high ON/OFF ratio, and good orthogonality. In this study, to screen for high-performance SWTs, we linked a series of algorithm-generated SWT sequences to the reporter gene 3WJdB and analyzed their performance using an *in vitro* transcription system (Figure 2A). In the absence of trigger RNA (OFF state), a small amount of the reporter gene (3WJdB) may still be transcribed. The fluorescent signal generated by the transcribed 3WJdB binding to DFHBI-1T is referred to as the leakage value. A low leakage value indicates that the SWT structure is stable and can effectively block the elongation of T7 RNAP, thereby strongly repressing downstream gene expression. The ON/OFF ratio refers to the fluorescence activation signal in the presence of trigger RNA (ON state) divided by the leakage fluorescence signal in the absence of trigger RNA (OFF state). A high ON/OFF ratio indicates that SWT can significantly enhance downstream gene expression in the ON state, demonstrating strong activation capability.

In this study, the fluorescence signals of 21 algorithm-generated SWT variants (The secondary structure predictions are shown in Figure S3) were measured under two different states, with both SWT sensor and trigger concentrations set at 10 nM. The fluorescence in the OFF state reflects the transcription termination efficiency of these 21 SWTs. Among them, JS5, JS6, JS8, JS9, and ZS17 exhibited high leakage fluorescence, indicating that their ability to inhibit T7 RNAP was weak and ineffective in blocking downstream gene transcription. In contrast, JS2, ZS1, ZS6, ZS19, and ZS22 exhibited minimal leakage expression, suggesting that the nucleotide distribution in these five SWT sequences maintained stable stem-loop structures, leading to effective transcriptional repression (Figure S4A). The fluorescence in the ON state reflects the transcriptional activation upon the addition of the complementary trigger RNA. Compared to the OFF state, JS2, ZS1, ZS16, ZS19, and ZS22 displayed a significant fluorescence signal output after adding the homologous trigger RNA, indicating that the base-pairing between sensor RNA and trigger RNA effectively disrupted the stem-loop structure, allowing T7 RNAP to proceed with transcription and activate downstream gene expression (Figure S4B). Additionally, we calculated the ON/OFF ratio for these 21 SWT variants (Figure 2B). JS2, ZS1, ZS16, ZS19, and ZS22 exhibited high ON/OFF values, with fluorescence activation levels of 10.41-fold, 17.71-fold, 18.52-fold, 22.21-fold, and 6.47-fold, respectively, upon the addition of the homologous trigger RNA, demonstrating effective transcriptional regulation. Although ZS17 exhibited the highest activation fluorescence intensity, its high leakage expression resulted in a relatively low ON/OFF ratio. To further validate the *in vivo* transcriptional regulatory capabilities of these five high-performance SWT variants, recombinant plasmids were constructed (Figure 2C) and tested in *E. coli* BL21(DE3) (Figure 2D). A plasmid containing only the 3WJdB reporter gene was used as a positive control. When an SWT was inserted, the fluorescence signal *in vivo* significantly decreased, indicating that the SWT could repress transcription in *E. coli* (OFF state). Upon the presence of trigger RNA, transcription activation levels of ZS1, JS2, ZS16, ZS19, and ZS22 were 2.82-fold, 2.41-fold, 2.00-fold, 9.13-fold, and 5.89-fold, respectively. Since the intracellular environment is more complex than the *in vitro* transcription system, multiple influencing factors (e.g., growth variability, cellular exclusion mechanisms, RNA degradation) may cause discrepancies between *in vitro* and *in vivo* results. However, our findings confirm that these five SWT variants also exhibit significant transcriptional activation effects in *E. coli*.

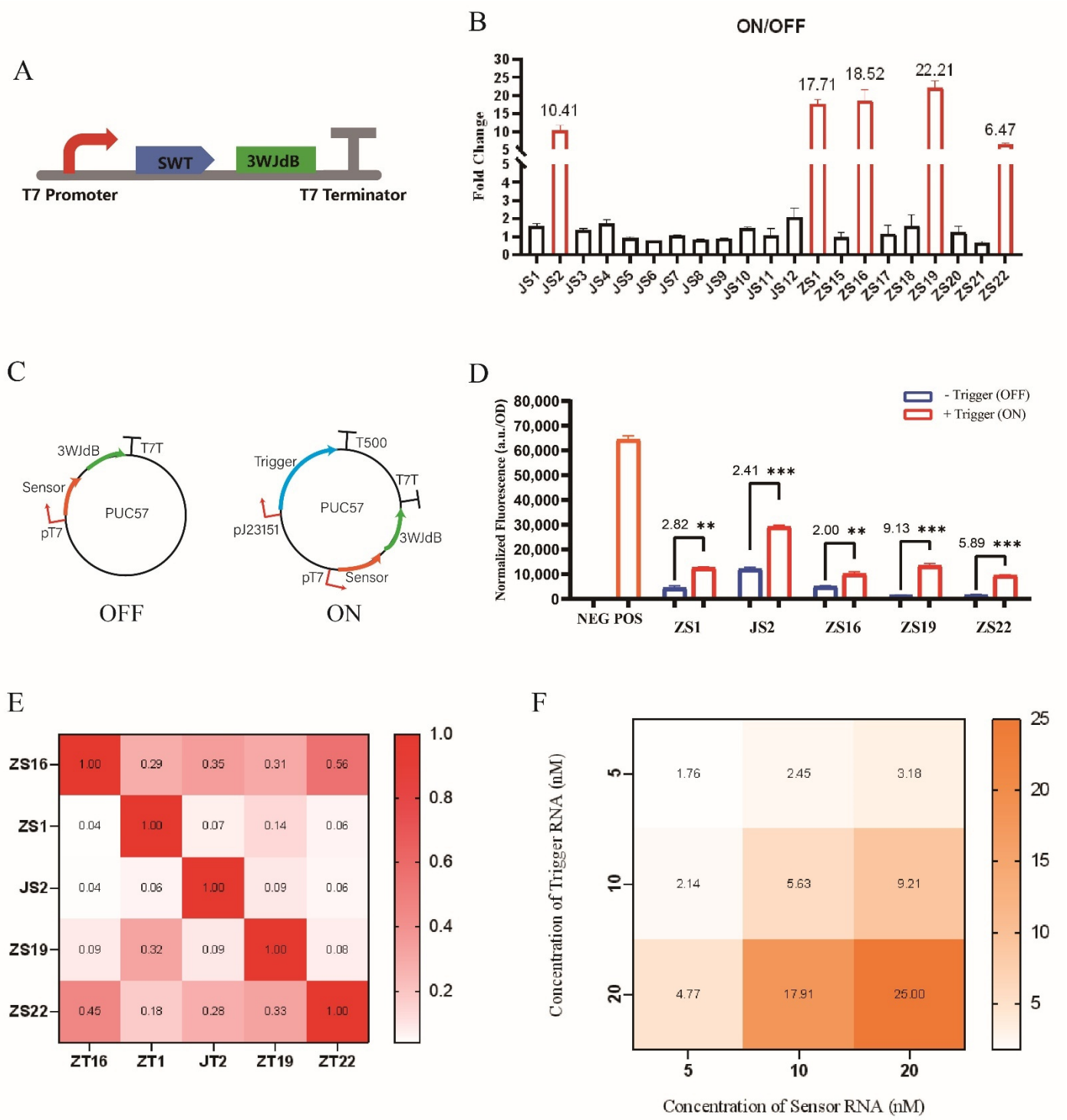

Figure 2. (**A**) Construction of linear DNA for *in vitro* transcription: The linear DNA sequence consists of a T7 promoter, SWT, reporter gene 3WJdB, and a T7 terminator. (**B**) ON/OFF ratio measurement. (Here, ZS refers to the SWT sensor previously studied by Zhao et al. JS refers to the SWT sensor previously studied by Jiao et al. The same applies hereafter). (**C**) Recombinant plasmid construction [49]: The OFF-state plasmid contains a T7 promoter, sensor RNA, 3WJdB, and a T7 terminator. The ON-state plasmid includes a constitutive promoter (J23151) driving the transcription of trigger RNA and an inducible T7 promoter regulating the transcription of sensor RNA. (**D**) The testing results in *E. coli* BL21(DE3). (**E**) Orthogonality analysis: The horizontal axis represents the triggers of the five candidate SWTs, and the vertical axis represents their corresponding sensors. The element in the i-th row and i-th column where $1 \leq i \leq 5$ indicates the fold change resulting from the binding of homologous SWT sensors and triggers, reflecting the specificity between each homologous sensor-trigger pair. These values are normalized and set to 1. The element in the i-th row and j-th column where $1 \leq i \leq 5$, $1 \leq j \leq 5$, and $i \neq j$ represent the fold change from non-homologous sensor-trigger binding, reflecting the degree of crosstalk between non-homologous SWT sensor-trigger pairs. These values are normalized as Fold Change$_{(i,j)}$/Fold Change$_{(i,i)}$. Thus, the diagonal represents the "homologous response", which should show a strong signal (darker color), while the off-diagonal elements represent "non-homologous responses", which are expected to be weak (lighter color). Experiment setup: Plasmid-sensor final concentration 1.5 nM; Linear DNA-trigger final concentration 20 nM. (Here, ZT

refers to the SWT trigger previously studied by Zhao et al. JT refers to the SWT trigger previously studied by Jiao et al. The same applies hereafter.) (**F**) Fold change under varying sensor and trigger RNA concentrations. For data in (**D**), *t*-tests were performed on each construct; ** $p < 0.01$ and *** $p < 0.001$ indicate the fluorescence change is statistically significantly different. Error bars represent the standard deviation (s.d.) of three biological replicates. Error bars indicate the average value of three independent biological replicates ± s.d.

Next, we predicted and evaluated the orthogonality of the five high-performance SWT sequences. Using the NUPACK online software (Version 3.1.0), we simulated the orthogonality of these five SWT pairs by analyzing the equilibrium concentrations of complexes and base pairing in the test tube ensemble (with both trigger RNA and sensor RNA set to 10 nM). The simulation results indicated that the homologous trigger and sensor RNA pairs were mutually orthogonal (Figure S5). We then conducted *in vitro* transcription experiments to verify their orthogonality (Figure 2E, with the fold change of homologous groups set to 1). The experimental results were largely consistent with the software predictions, with the exception of ZS16 and ZS22, which exhibited slightly weaker orthogonality, suggesting that some crosstalk might exist between their non-homologous trigger and sensor RNAs. Nevertheless, the overall orthogonality was well maintained. To further investigate the regulatory mechanism of SWT and optimize its regulatory efficiency, we selected ZS1 as a representative and explored the effects of different concentrations of trigger RNA and sensor RNA on *in vitro* transcription. Meanwhile, to further investigate the regulatory mechanism of SWT and optimize its regulatory efficiency, we used ZS1 as an example to examine the effects of *in vitro* transcription under different concentrations of SWT trigger and sensor. Through experiments, we measured the Fold Change under conditions where the SWT sensor and trigger concentrations were 5 nM, 10 nM, and 20 nM, respectively. (Figure 2F). On one hand, an increase in trigger concentration at a fixed sensor concentration led to greater activation efficiency. When the ZS1 sensor concentration was 20 nM, the fold change was 3.18-fold (5 nM trigger), 9.21-fold (10 nM trigger), and 25-fold (20 nM trigger). This could be attributed to the higher trigger concentration enhancing its binding with the sensor, leading to a more extensive disruption of the sensor stem-loop structure. As a result, more T7 RNAP molecules can continue transcription, producing higher amounts of 3WJdB, which binds to DFHBI-1T and generates a stronger fluorescence signal, thereby enhancing activation efficiency. On the other hand, at a fixed trigger concentration, the activation fold change also increased with rising sensor concentrations. When the trigger concentration was 20 nM, the fold change reached 4.77-fold (5 nM sensor), 17.91-fold (10 nM sensor), and 25-fold (20 nM sensor). This may be due to the fact that at low sensor concentrations, some of the transcribed trigger molecules fully bind with the available sensor, leading to an excess of unbound triggers. This saturation state could increase the burden on the transcription system or introduce non-specific binding signals. As the sensor concentration increases, the efficiency of trigger utilization improves, further enhancing activation. These findings confirm our analysis, demonstrating that transcription efficiency positively correlates with both the sensor and trigger concentrations within a certain concentration range.

3.2. SWT Cascade Reaction Construction and Expansion

To achieve stepwise signal processing and dynamic transmission, we constructed a cascade reaction loop *in vitro* using SWT, which enables the output signal of one level to serve as the input signal for the next level, facilitating signal transmission. Multiple layers are connected to drive several modules to work together for dynamic regulation. The construction of a multi-layer cascade regulation loop not only increases the functionality of biological circuits, enabling multi-level dynamic regulation that can simulate advanced biological processes, but it also amplifies the signal, reduces background noise, and stabilizes the signal output. Each layer can serve as a gatepoint, ensuring that the next level's response is only triggered under specific signal conditions, thereby functioning as a layered decision-making mechanism.

Previously, we constructed a 3-level cascade loop *in vitro* based on SWT. In this study, after confirming the orthogonality of the five SWT sequences (ZS1, JS2, ZS16, ZS19, and ZS22), we extended the cascade reaction loop to 6 levels. This was achieved by replacing the fluorescent reporter gene 3WJdB, the output module after the SWT, with the trigger RNA of the next level, thereby enabling multi-level regulation. The detailed construction strategy is shown in Figure 3A. The entire regulatory network is divided into three modules: the signal input module (X), the signal conversion module (Y), and the signal output module (Z). The trigger RNA ZT1 transcribed by the input module is responded to by the second-level signal conversion module, where it binds with ZS1-ZT16, disrupting the hairpin structure of ZS1, allowing downstream gene ZT16 to be successfully transcribed. This process continues with responses from subsequent levels until the final signal conversion module outputs ZT19. Finally, ZT19 is responded to by the signal output module ZS19-3WJdB, binding and disrupting the hairpin structure of ZS19, allowing the reporter gene 3WJdB to be successfully transcribed, producing and releasing fluorescence after binding to the fluorescent molecule.

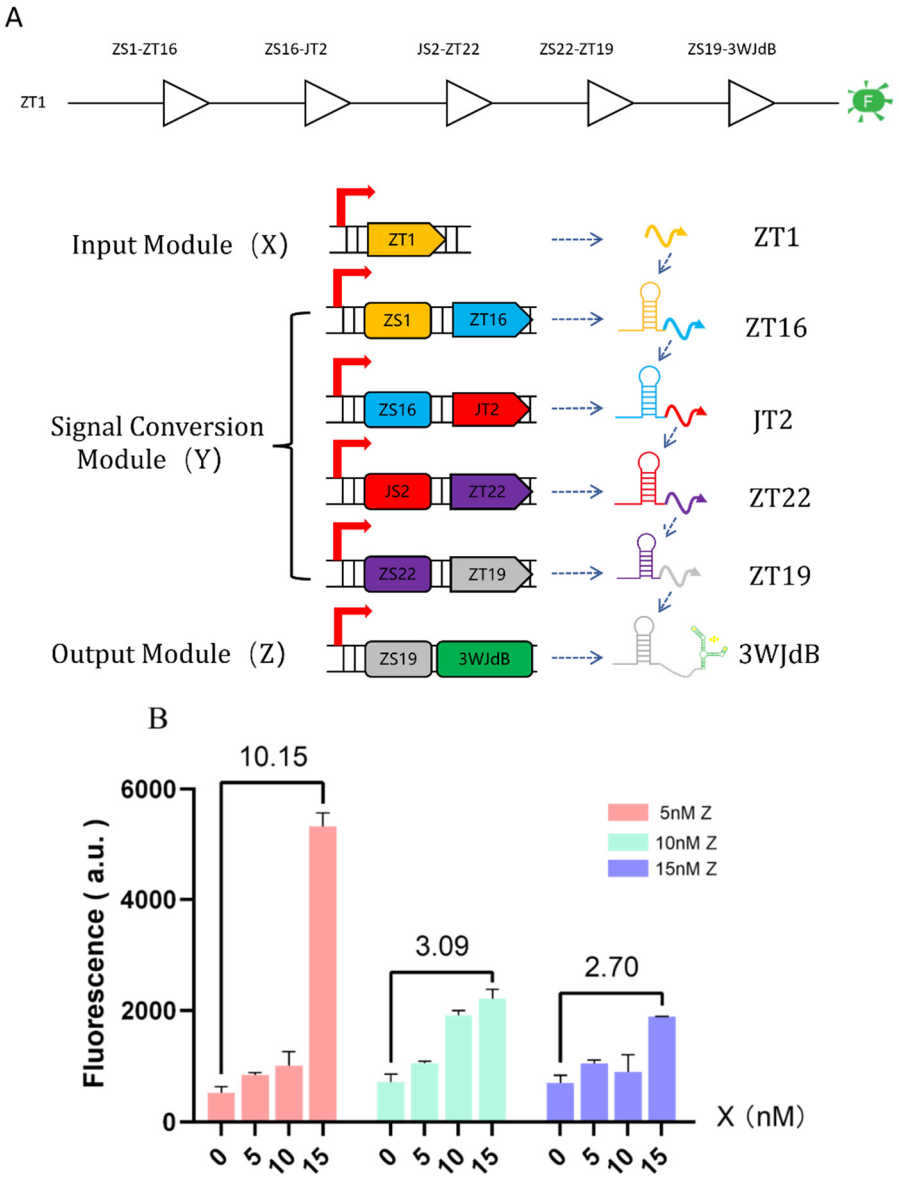

Figure 3. (**A**) Construction of the multi-level cascade reaction circuit: The entire cascade reaction circuit is divided into three modules: input module (X), conversion module (Y), and output module (Z). (**B**) Six-level cascade *in vitro* transcription test: The concentration of templates in the signal conversion module Y is fixed at 5 nM (to simplify the variable space and stabilize the transcription system, ensuring effective transcription of other modules and allowing us to focus on the effect of cascade layer number on signal amplification). The transcription conditions are tested with input module X concentrations of 0, 5, 10, and 15 nM, and output module Z concentrations of 5, 10, and 20 nM. Error bars indicate the average value of three independent biological replicates ± s.d.

Due to the limitations of the raw materials in the *in vitro* transcription system, the DNA templates that can be transcribed are also limited. To reduce the load on the transcription system, we fixed the concentration of the signal conversion module at 5 nM for all four layers and characterized the signal input and output modules at different concentrations. We co-transcribed the six linear DNA templates of the entire cascade regulation model in the same transcription system (one-pot method). The results show that when the concentration of the signal input module X is 15 nM, the concentration of the conversion module Y is 5 nM, and the concentration of the signal output module Z is 5 nM, the cascade reaction exhibits a maximum fluorescence activation of 10.15 times (Figure 3B). Interestingly, we observed that when the concentration of the input module X was 15 nM, and the concentration of each signal conversion module Y was 5 nM, the final fluorescence output decreased as the concentration of the signal output module Z increased, showing a negative correlation. We hypothesize that this phenomenon may be due to two main factors. First, at high concentrations, the DNA template of the output module may competitively bind to T7 RNA polymerase, impeding the overall signal transduction process and leading to reduced fluorescence output. Second, the output module contains a structurally complex reporter gene, which is more prone to misfolding under high concentration conditions,

thereby reducing the efficiency of fluorescent dye binding and leading to lower fluorescence signals. Additionally, as the total template concentration increases in the system, the transcription machinery becomes overburdened, and resources are depleted, which may further contribute to fluorescence signal degradation or transcriptional inhibition. Furthermore, we analyzed the real-time fluorescence under the optimal reaction conditions, and the entire cascade reaction was very rapid, reaching its peak in 30 min. Afterward, the fluorescence signal gradually faded due to the consumption of raw materials in the transcription system and crosstalk between templates (Figure S6A). To reduce crosstalk between templates and ensure complete transcription of the reporter gene, we also attempted to co-transcribe the signal input and conversion modules in the same system while transcribing the signal output module in a separate transcription system (Two-pots). Both systems were incubated at 37 °C for 30–45 min to accumulate a certain amount of RNA before being mixed into the same system to bind with the fluorescent molecule DFHBI-1T. The results showed that the real-time fluorescence no longer exhibited a decreasing trend, indicating that the transcription system limitation was improved to some extent. Still, the reaction process was very slow, with the maximum activation only reaching 1.26 times (Figure S6B,C). The effect was much weaker than the one-pot method, possibly because placing the entire cascade reaction in the same transcription system allows the signal transmission to be more synchronized, efficient, and precise, leading to a faster system response.

3.3. Construction and Characterization of the SWT Biological Logic Gate

Biological logic gates introduce the concept of electronic logic gates and are functional elements and systems that perform logical operations in biological systems. These gates generate specific outputs based on input signals under certain conditions (e.g., concentration, enzyme activity, temperature, or other environmental factors). Previous research combined SWT with Toehold Switches to construct an AND gate that jointly regulates transcription and translation. Additionally, a two-input, three-layer OR gate was constructed by combining cascade reactions with the OR gate. In this study, we used a fluorescent aptamer as a reporter gene and constructed four new basic biological logic gate control circuits *in vitro* to achieve more flexible and precise control over the transcription process while expanding the logic operation capabilities of SWT.

3.3.1. AND Gate

The AND gate is characterized by producing an output signal (output is 1) only when both input signals are present simultaneously (*i.e.*, both inputs are 1). The construction of the AND gate involves combining two different SWTs to form two stem-loop structures that block transcription. Only when both homologous Trigger RNAs are present can these stem-loop structures be fully disrupted, allowing transcription to proceed normally (Figure 4A). To experimentally validate the functionality of this model, we assembled the AND gate by linking ZS22 and ZS19 SWTs together. We tested its performance through *in vitro* transcription (with all template concentrations set at 10 nM). The results showed that no significant fluorescence signal activation was observed when no input was present, only a single input of ZT22, and only a single input of ZT19. However, when both ZT22 and ZT19 were present as inputs, there was a 6.67-fold increase in fluorescence activation compared to the absence of any input (Figure 4B). This confirms the functionality of the AND gate model.

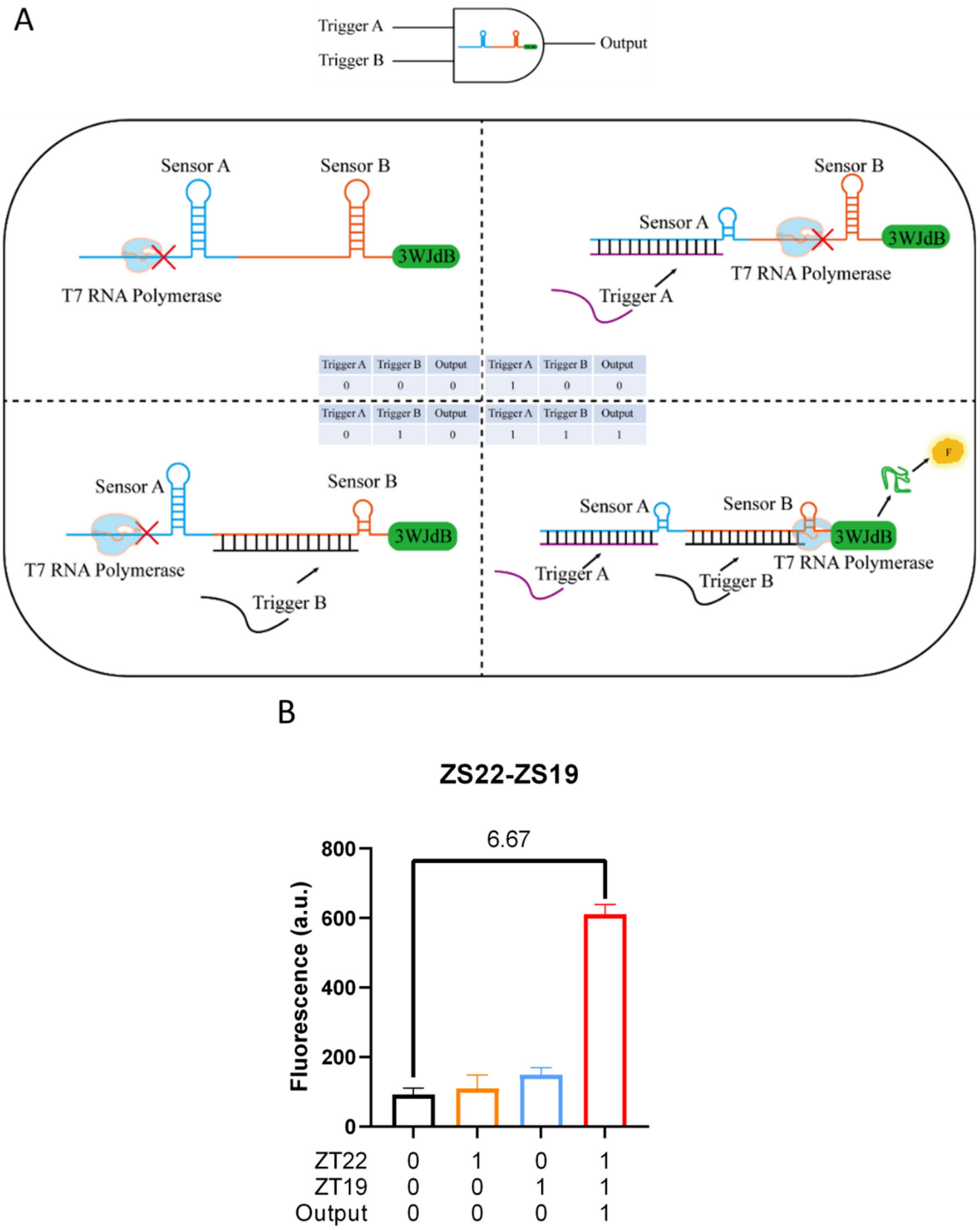

Figure 4. Construction and characterization of the AND gate. (**A**) Construction and mechanism: Two different SWTs are linked in series to form two independent stem-loop structures. Only when both homologous trigger RNAs of these two different SWTs are present simultaneously can these stem-loop structures be fully disrupted, leading to a large fluorescence output. (**B**) Performance characterization: The AND gate was constructed using ZS22 and ZS19 as examples, and *in vitro* transcription was tested with all template concentrations set at 10 nM. When both homologous trigger RNAs from the two different SWTs were present, a 6.67-fold fluorescence activation was observed. Error bars indicate the average value of three independent biological replicates ± s.d.

3.3.2. NOT Gate

The NOT gate functions oppositely to the SWT, characterized by having signal output (output is 1) when no input signal is present (input is 0) and having no signal output (output is 0) when signal input is present (input is 1). The construction of the NOT gate model involves introducing a sequence (referred to as the "Anti-Toehold-Stem", ATS) in front of the SWT that is complementary to the SWT's toehold and upper stem regions, thereby disrupting the SWT

structure. This causes the SWT to switch from a default open state (no fluorescence output) to a default closed state (fluorescence output), enabling signal output even without input. Subsequently, an input trigger RNA sequence (referred to as the "Anti-Anti-Toehold-Stem", AATS) is introduced, which preferentially binds to the ATS sequence, allowing the previously disrupted SWT structure to recover and block transcription (Figure 5A). We constructed a NOT gate using ZS19 as an example and experimentally validated the functionality of the NOT gate model (where the concentration of input Trigger RNA template DNA was 20 nM, and the concentration of Sensor RNA template DNA was 10 nM). The results showed that when there was no input, a large fluorescence signal was output, while the fluorescence signal was significantly reduced when the input was present, indicating a switch from the default closed state to the open state, suppressing transcription and significantly reducing the fluorescence signal output to near zero (Figure 5B).

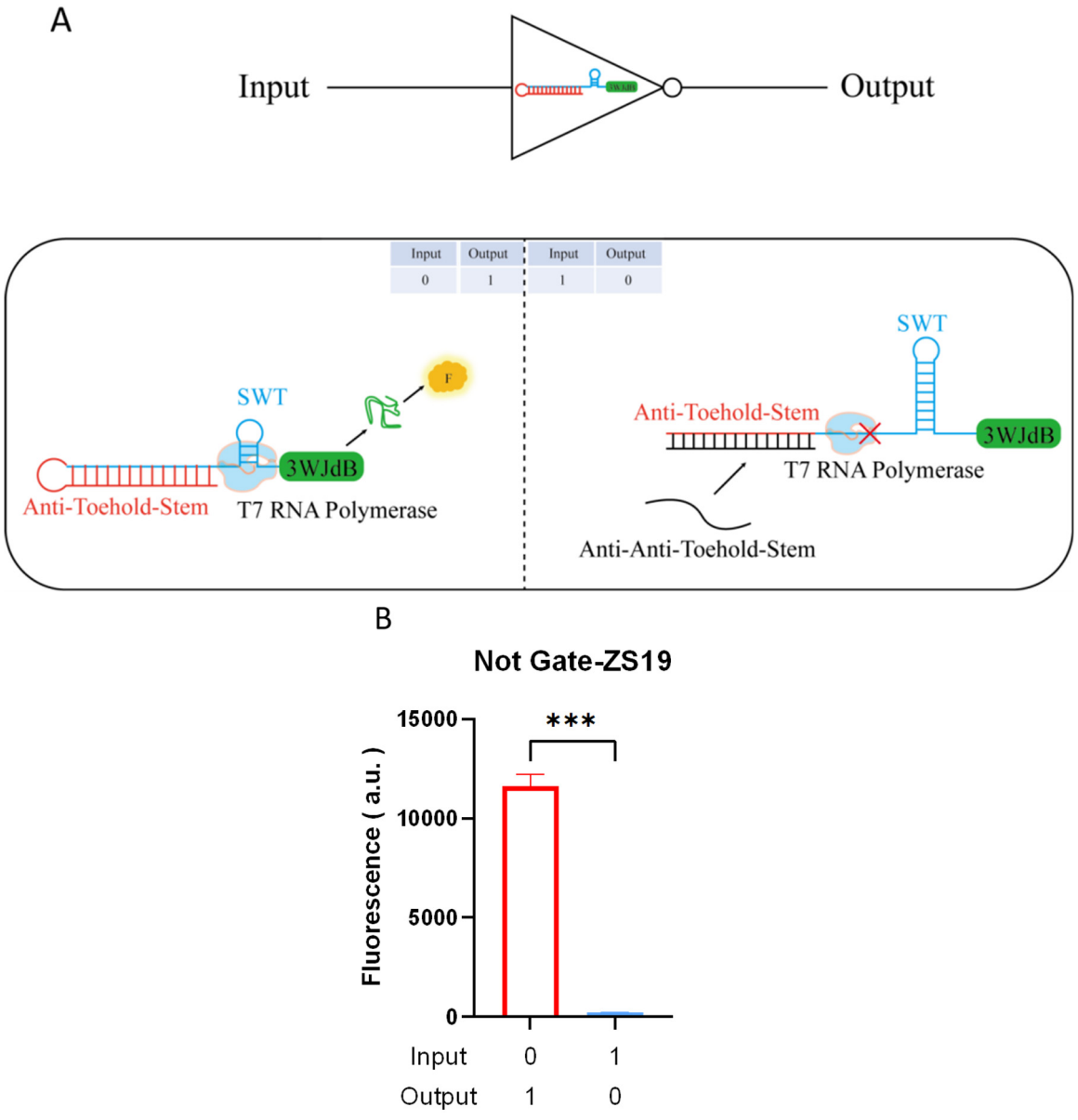

Figure 5. Construction and characterization of the NOT gate. (**A**) Construction and mechanism: By introducing an ATS sequence before the SWT, the original hairpin structure of the SWT is shielded. In the absence of a Trigger introduction, the state switches from default open to default closed, resulting in fluorescence signal output. However, when the Trigger (AATS sequence) is introduced, AATS competes with ATS for binding, allowing the SWT structure to recover and properly terminate transcription, leading to no fluorescence signal output. (**B**) Performance characterization: The NOT gate was constructed using ZS19 as an example, with the Sensor template concentration set to 20 nM. In the absence of Trigger (AATS), a large fluorescence signal was output. When the Trigger template concentration of 10 nM was introduced, the fluorescence signal significantly decreased. For data in (**B**), *t*-tests were performed on each construct; *** $p < 0.001$ indicates the fluorescence change is statistically significantly

different. Error bars represent the standard deviation (s.d.) of three biological replicates. Error bars indicate the average value of three independent biological replicates ± s.d.

3.3.3. NAND Gate

The NAND gate functions oppositely to the AND gate, being a combination of the AND gate and the NOT gate. Its characteristic is that, in the absence of input signals or with only one input signal, a fluorescence signal is output (output is 1); however, when both input signals are present simultaneously, no signal is output (output is 0). After validating the functionalities of the AND gate, NOT gate, and cascade reaction models, we combined their construction strategies and ideas to develop the NAND gate. The NAND gate regulatory circuit is essentially a three-layer cascade reaction. The first layer is the input module (input trigger RNA), the second layer is a signal conversion module controlled by an AND gate (sensor A-sensor B-AATS), and the third layer is a signal output module controlled by a NOT gate (ATS-sensor C-3WJdB). By replacing the reporter gene 3WJdB in the AND gate model with the AATS sequence, the system ensures that only when both trigger RNAs from the two SWTs (sensor A and sensor B) are present will the AATS sequence be transcribed. This sequence will then act as the input for the NOT gate, binding with the ATS sequence in the output module. When the first layer has no input or only one input, the second-layer conversion module will not transcribe the AATS sequence, preventing it from binding with the ATS sequence in the output module, thus allowing normal transcription. However, when both inputs (trigger A and trigger B) are present in the first layer, both hairpin structures (sensor A and sensor B) in the second layer will be destroyed, allowing the downstream gene AATS sequence to be transcribed. This sequence will serve as the input for the third-layer output module, binding with the ATS sequence, which restores the original conformation of the SWT (sensor C) secondary structure and blocks the transcription of the reporter gene 3WJdB, leading to a false output (Figure 6A).

We used the ZS1, JS2, and ZS19 to validate the NAND gate model. The first layer consisted of the input modules ZT1 and JT2, the second layer was the signal conversion module ZS1-JS2-AATS19, and the third layer was the signal output module ATS19-ZS19-3WJdB. The input module template DNA concentration was 20 nM, while the template DNA concentrations of the signal conversion and output modules were both 10 nM. These three modules were co-transcribed for testing. The results showed that when there was no input, or when only ZT1 or JT2 was input, or when both ZT1 and JT2 were input, there was a significant fluorescence signal output (Figure S7). This did not align with the NAND gate logic, possibly due to template interference, complex secondary structures, or overloading in the transcription system. To address this, we improved the experimental method by transcribing the signal output module in a separate transcription system to ensure the reporter gene 3WJdB had enough energy and material to transcribe and fold properly without interference. The input and conversion modules were co-transcribed in another system. Both systems were incubated at 37 °C for 30–45 min to accumulate enough RNA, which was then mixed in the same system and tested for fluorescence with the fluorescent molecule DFHBI-1T. The results showed that when both ZT1 and JT2 were input, the fluorescence signal significantly decreased compared to conditions where no input, only ZT1, or only JT2 were used, which is more in line with NAND gate logic. However, when both input signals were simultaneously present, a substantial fluorescence signal was still observed, indicating that the system failed to realize the ideal “NAND” logic fully. We speculate that this may be due to insufficient concentrations of the Triggers or suboptimal binding kinetics with the Sensor, resulting in incomplete formation of the terminator structure and subsequent readthrough transcription. The simultaneous presence of two Triggers may also introduce new RNA-RNA folding pathways or intermediate conformations, thereby altering the original SWT termination mechanism and leading to unintended or partial activation. Additionally, in the *in vitro* transcription system, transcriptional resources such as RNA polymerase and NTPs may be competitively consumed, contributing to non-ideal fluorescence output (Figure 6B).

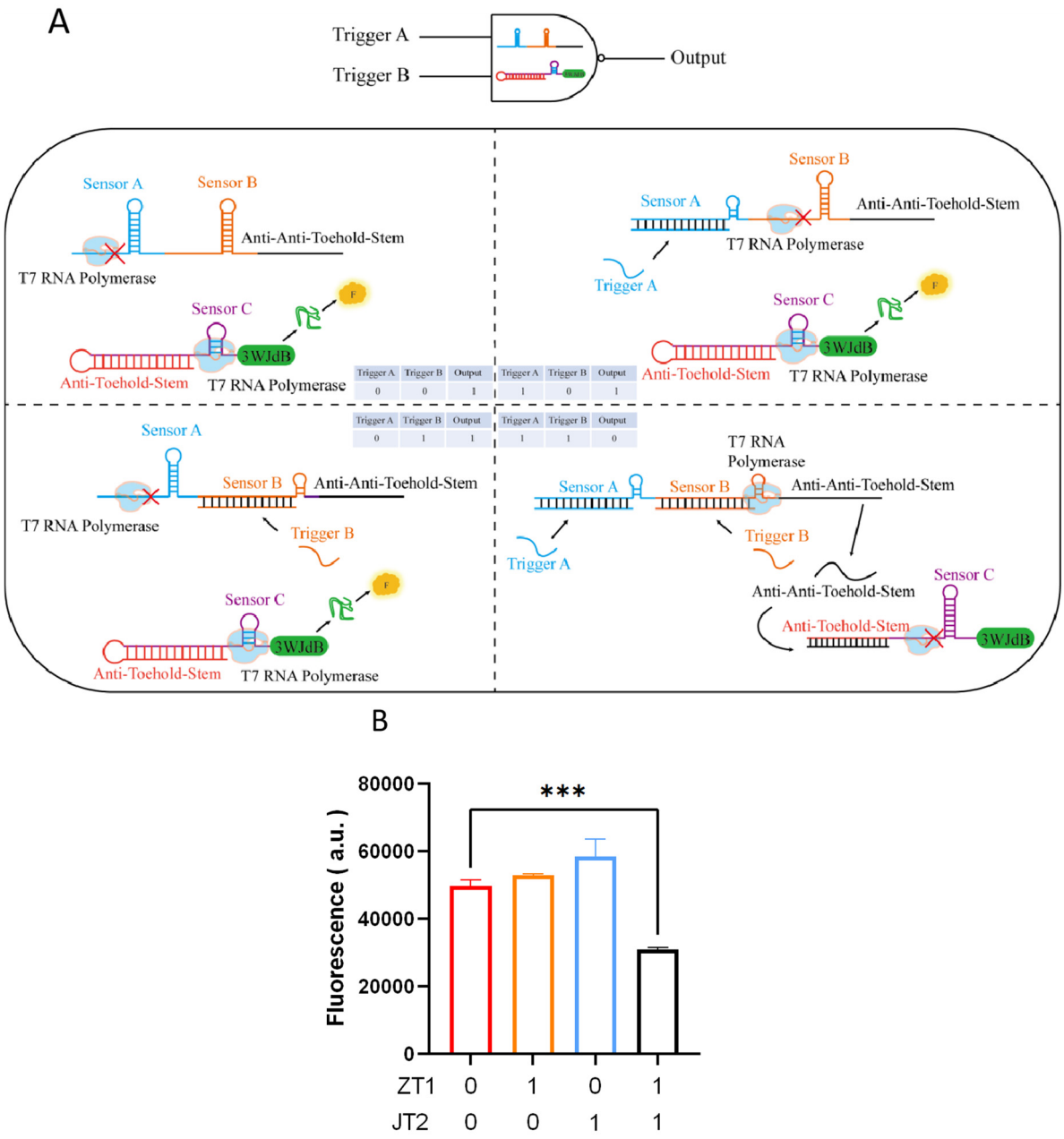

Figure 6. Construction and characterization of the NAND gate. (**A**) Construction and mechanism: This model is essentially a cascade reaction loop involving three switchable transcription terminators (SWTs). The input module consists of input triggers (ZT1 and JT2). The second-layer signal conversion module is formed by two SWT sequences in series to construct an AND gate (ZS1-JS2-AATS19). The signal output module is formed by a third SWT, which constructs a NOT gate (ATS19-ZS19-3WJdB). The transcription module is only activated when both input triggers, ZT1 and JT2, are present, leading to the output of the AATS sequence, which then interacts with the NOT gate in the output module, resulting in a decrease in output fluorescence. (**B**) Performance characterization: The template concentration for input modules ZT1 and JT2 is 20 nM, while the template concentration for the signal conversion module ZS1-JS2-AATS19 and the output module ATS19-3WJdB is 10 nM. The input and signal conversion modules are co-transcribed, while the output module is transcribed separately. After 30–45 min of reaction, the modules are mixed into the same system and incubated with DFHBI-1T. When both ZT1 and JT2 are input together, the output fluorescence significantly decreases. For data in (**B**), *t*-tests were performed on each construct; *** $p < 0.001$ indicates the fluorescence change is statistically significantly different. Error bars represent the standard deviation (s.d.) of three biological replicates. Error bars indicate the average value of three independent biological replicates ± s.d.

3.3.4. NOR Gate

The NOR Gate is characterized by the absence of an output signal (output is 0) whenever any input signal is present. The design of the NOR gate is similarly inspired by the construction principles of the AND and NOT gates. By

combining two NOT gates, the model ensures that no signal output is generated as long as either NOT gate is active (Figure 7A).

We constructed the NOR gate using ZS19 and JS2, with the AATS sequences of ZS19 and JS2 serving as the two inputs. The DNA template concentrations were as follows: the signal output module ATS A (ZS19)-ZS19-AATS B (JS2)-JS2-3WJdB was set at 10 nM, while the input modules AATS A (ZS19) and AATS B (JS2) were set at 20 nM. Analysis of the results showed that a high fluorescence signal was observed in the absence of any input signals. However, when either AATS A (ZS19) or AATS B (JS2) was present, fluorescence significantly decreased, and when both were input simultaneously, the fluorescence signal was nearly zero (Figure 7B). These results indicate that the NOR gate model functions as expected.

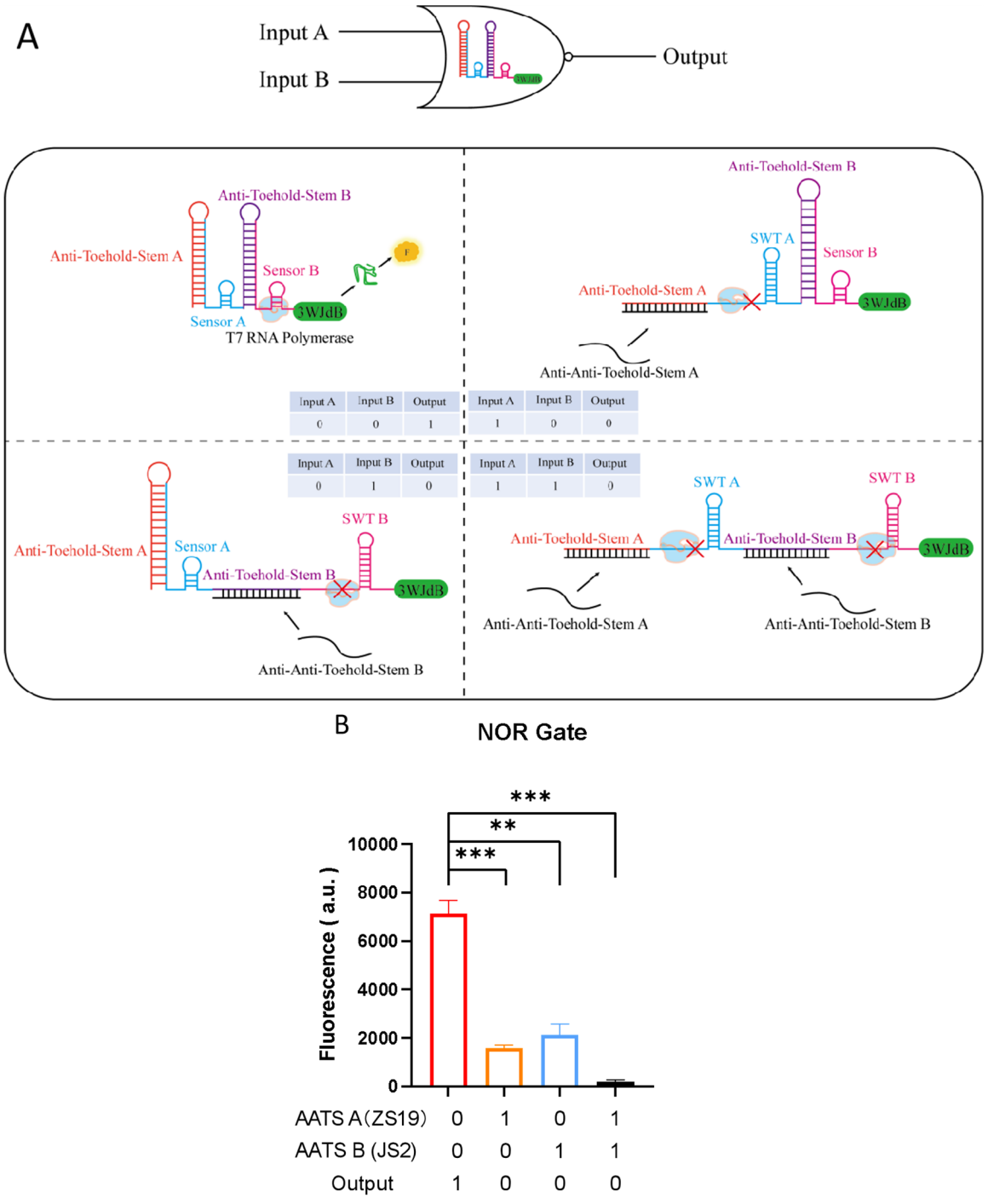

Figure 7. Construction and characterization of the NOR Gate. (**A**) Construction and mechanism: Using ZS19 and JS2 as examples, individual NOT gates were constructed. By combining these two NOT gates, the NOR gate was established. In the absence of any input (AATS sequences), the structure of the switchable transcription terminators (SWTs) remains masked, allowing transcription to proceed and resulting in fluorescence output. However, when either AATS sequence is introduced, the corresponding SWT restores its original structure, terminating transcription. When both AATS sequences are input simultaneously, transcription

termination is further enhanced. (**B**) Performance characterization: The signal output module ATS A (ZS19)-ZS19-ATS B (JS2)-JS2-3WJdB was set at a DNA template concentration of 10 nM, while the input modules AATS A (ZS19) and AATS B (JS2) were set at 20 nM. In the absence of any input, the SWT structures remain masked, enabling normal transcription and resulting in high fluorescence output. When either AATS sequence is introduced, the corresponding SWT regains its original structure, inhibiting transcription and significantly reducing fluorescence output. When both AATS sequences are present, transcription termination is further enhanced, leading to an even lower fluorescence signal. For data in (**B**), *t*-tests were performed on each construct; ** $p < 0.01$ and *** $p < 0.001$ indicate the fluorescence change is statistically significantly different. Error bars represent the standard deviation (s.d.) of three biological replicates. Error bars indicate the average value of three independent biological replicates ± s.d.

3.4. Aptamer-Based Transcriptional Regulation

Due to the high specificity between nucleic acid aptamers and their ligands and the conformational changes induced upon ligand binding that can disrupt downstream gene expression, nucleic acid aptamers can be developed as novel transcriptional regulatory elements. The thrombin aptamer is well-suited for constructing synthetic regulatory models due to its well-established research foundation, clearly defined structural characteristics [50], high specificity, and strong binding affinity. Moreover, thrombin is not endogenously expressed in cell-free systems or most non-mammalian biological systems, resulting in minimal background interference [51,52]. Therefore, in this study, we selected the thrombin aptamer as a functional regulatory element and inserted it into a transcriptional regulatory circuit to evaluate its potential for transcriptional control. Here, we selected four different thrombin aptamers and predicted their secondary structures (Figure S8A) and three-dimensional interactions with the thrombin protein (Figure S8B) using Mfold and AlphaFold3. Based on the reliability of the predictions, molecular docking visualization was performed for TBA25, TBA15, and TBA29. The results showed that TBA25, TBA15, and TBA29 interacted with the thrombin protein at 10, 3, and 2 nucleotide sites, respectively (Figure S8C), suggesting that TBA25 may have the highest binding affinity for its ligand. To experimentally characterize the binding affinities of these four candidate aptamers, we conducted circular dichroism (CD) spectroscopy analysis (Figure S9). The CD spectrum of TBA25 exhibited a global downward shift upon ligand binding, indicating that its conformation became significantly more relaxed. This structural change is expected to facilitate transcription activation. While TBA15, TBA29, and TBA61 are DNA aptamers, TBA25 is an RNA aptamer.

To experimentally verify the regulatory effects of these aptamers on transcription, we performed *in vitro* transcription assays. First, to eliminate potential interference from the ligand itself, we confirmed that varying concentrations of thrombin had no significant impact on transcription (Figure S10). Next, we inserted the four aptamers at different positions upstream and downstream of the T7 promoter in linear DNA constructs, using 3WJdB linear DNA as the positive control. The transcriptional regulatory effects were analyzed by comparing transcription levels in the presence and absence of thrombin (800 nM). Real-time fluorescence measurements over 2 h (Figure 8A–G) showed that TBA25 exhibited the strongest transcriptional activation effect, with the highest fluorescence peak after 2 h. Furthermore, fold change analysis (Figure 8H) indicated that inserting the DNA aptamer at different positions upstream or downstream of the promoter had no significant effect on transcriptional regulation. This suggests that aptamer insertion at these sites has little impact on promoter function and does not interfere with the recruitment of T7 RNA polymerase while still exerting a certain degree of transcriptional activation. The RNA aptamer TBA25 exhibited the strongest transcriptional activation effect, enhancing transcription levels by up to 1.61-fold upon ligand binding.

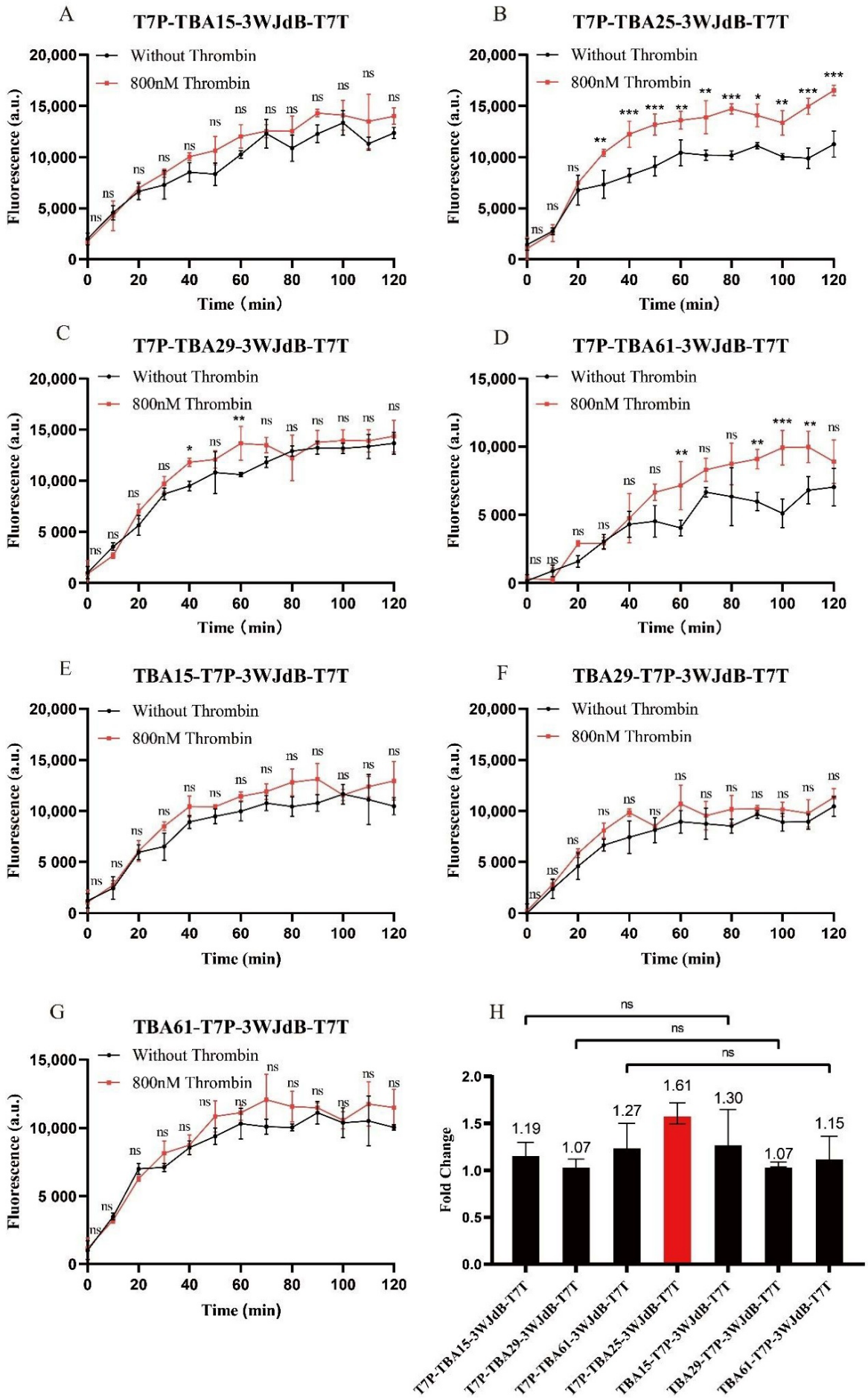

Figure 8. Characterization of aptamer-based transcriptional regulation. (**A**–**G**) Real-time fluorescence intensity curves over 2 h, showing the transcriptional activation effects of four different aptamers inserted at various positions upstream and downstream of

the T7 promoter. After adding 800 nM thrombin, fluorescence signals increased in all cases, indicating that aptamer-ligand binding positively influenced transcription. Among them, TBA25 exhibited the highest fluorescence peak after ligand binding, suggesting the strongest activation effect. (**H**) Fold Change analysis further confirms that TBA25 demonstrates the most significant regulatory effect on transcription among the tested aptamers. All sensor template concentrations were maintained at 10 nM. For data in (**A**–**G**), Two-way ANOVA was performed on each construct; * $p < 0.05$, ** $p < 0.01$, *** $p < 0.001$ indicate the fluorescence between the group without thrombin and the group of 800 nM thrombin are statistically significantly different, $p > 0.05$ indicates the difference is not statistically significant (ns). For data in (**H**), *t*-tests were performed on each construct, $p > 0.05$ indicates the fold change is not statistically significant (ns). Error bars indicate the average value of three independent biological replicates ± s.d.

3.5. Aptamer-SWT Transcriptional Co-Regulation

To expand the flexibility and programmability of transcriptional regulation using SWT and aptamer, and to construct an integrated regulatory and sensing genetic element, we attempted to combine aptamer with SWT to explore their synergistic regulatory effects on transcription. Using ZS1 as an example, we also investigated the effect of inserting the aptamer at different positions upstream and downstream of the promoter and the synergistic transcriptional regulation of the two genetic elements (with the template concentration of the sensor RNA module being 10 nM, the trigger RNA template concentration being 20 nM, and the ligand molecule Thrombin concentration being 800 nM). Analysis of the transcription results showed that when TBA15 was combined with ZS1, inserting TBA15 at different positions upstream or downstream of the promoter resulted in varying transcription effects. Insertion of TBA15 downstream of the promoter led to high leakage expression, and the introduction of Trigger RNA (ZT1) could not activate transcription. However, when TBA15 was inserted upstream of the promoter, leakage expression was low, and the introduction of Trigger RNA (ZT1) resulted in a 4.83-fold fluorescence activation. This suggests that inserting TBA15 upstream of ZS1 interfered with the proper folding of the ZS1 structure, causing an increase in leakage expression and preventing response to the trigger RNA. When TBA29 was combined with ZS1, inserting it at different positions upstream and downstream of the promoter produced two distinct selective response results: when TBA29 was inserted upstream of the promoter, it responded only to the Trigger RNA but not to the Ligand; when TBA29 was inserted downstream of the promoter, it primarily responded to the Ligand, with a lower response to the Trigger RNA. The combination of the RNA aptamer TBA25 with ZS1 showed the best synergistic effect, exhibiting the lowest leakage expression and the highest ON/OFF value under all input conditions. Compared to inputs of just the Trigger or Ligand, the synergistic regulation resulted in a 3.3-fold and 7.84-fold increase in activation, respectively (Figure 9).

In conclusion, we observed a synergistic regulatory effect between these two elements by combining aptamers and switchable transcription terminators (SWT) and comparing their transcriptional regulatory effects at different relative positions. Each element either promoted or inhibited transcription when acting alone, but when they acted together, they further enhanced transcription.

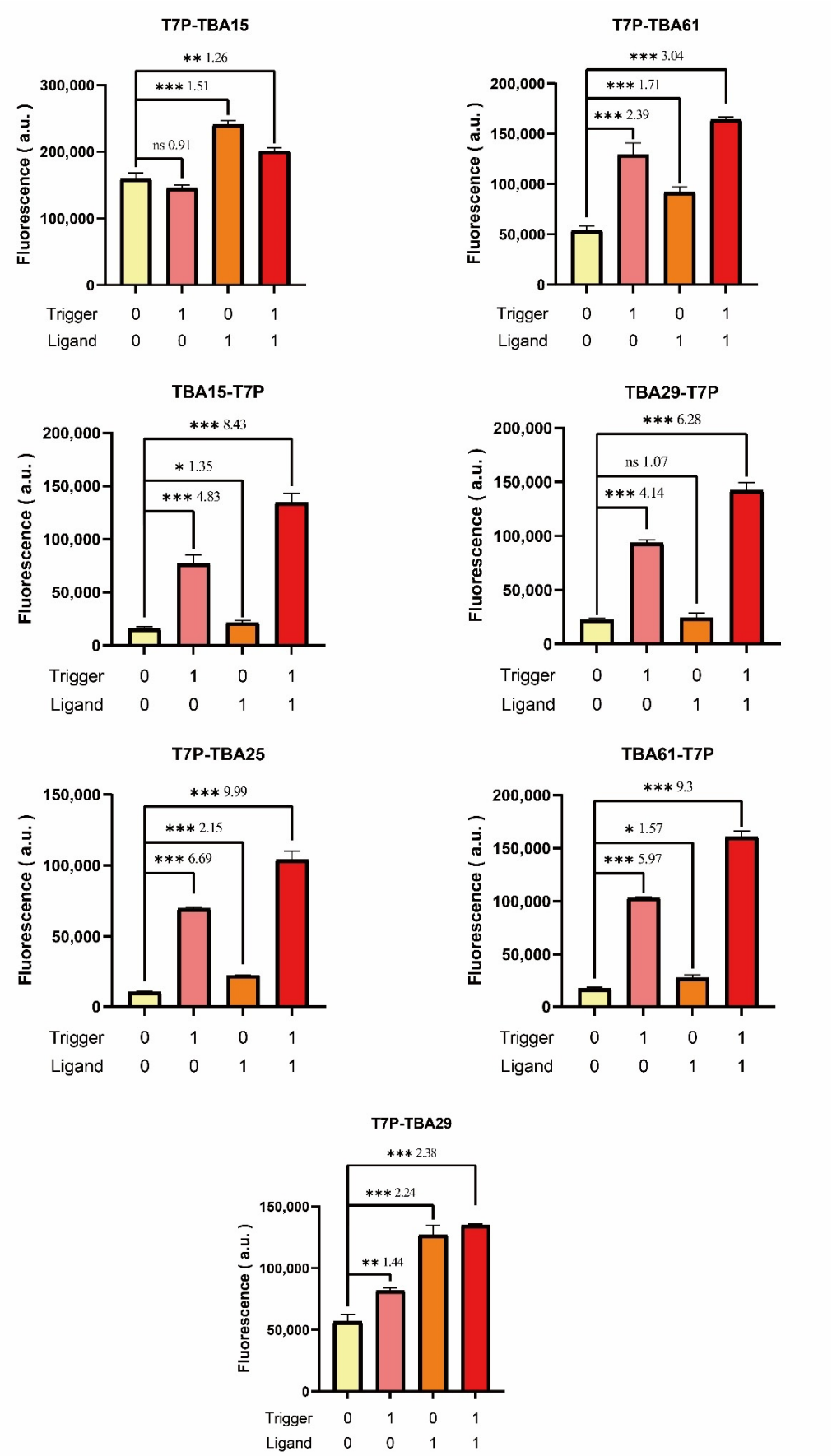

Figure 9. Characterization of the synergistic transcriptional regulation effect of Aptamer-SWT combination. We inserted the aptamer at different positions upstream and downstream of the T7 promoter and combined it with SWT (ZS1)-3WJdB-T7T to investigate its effect on transcriptional regulation (with the sensor template concentration at 10 nM, trigger template concentration at 20 nM, and thrombin concentration at 800 nM). After combining aptamer with SWT, a certain synergistic regulatory effect was observed. When the two elements acted alone, they either promoted or inhibited transcription; however, when they acted together,

they further enhanced transcription. Among the combinations, when TBA25 was combined with ZS1, it exhibited the lowest leakage expression. Compared to transcription activation effects when only the trigger or ligand was input, the activation fold increased by 3.3-fold and 7.84-fold, respectively, when both were input together. For data in the figure, *t*-tests were performed on each construct; * $p < 0.05$, ** $p < 0.01$, *** $p < 0.001$ indicate the fluorescence change is statistically significantly different, $p > 0.05$ indicates the fluorescence change is not statistically significant (ns). The numbers on the bars indicate the fold change values. Error bars indicate the average value of three independent biological replicates ± s.d.

3.6. Construction of Transcriptional Regulation Models Based on Aptamer-SWT Integration

To expand the response and integration of transcriptional regulatory circuits to input signals from different sources, achieve complex signal processing, and enhance the robustness and flexibility of regulatory circuits, this study combines aptamers and SWTs to construct biological logic gates and cascade reaction models with heterologous inputs.

3.6.1. Orthogonality Verification

First, to verify that the aptamer and SWT function orthogonally as distinct genetic elements, ensuring their compatibility, modularity, and independence in synthetic biological circuit design and gene regulation, we selected TBA25 and ZS1—both of which demonstrated good performance—for orthogonality validation. The experimental conditions were set as follows: SWT and aptamer template DNA concentrations at 10 nM, trigger RNA template concentration at 20 nM, and ligand concentration at 800 nM.

Figure 10A compares activated fluorescence peak values, while Figure 10B shows the percentage of activated fluorescence (with the activation fluorescence of homologous groups normalized to 1). The results indicate that the trigger and sensor of SWT exhibit absolute orthogonality, as the ligand molecule thrombin does not interfere with the sensor. However, a slight fluorescence activation was observed between the SWT trigger and the aptamer, possibly due to partial base complementarity between their sequences. Overall, the components of these two genetic elements exhibit good orthogonality.

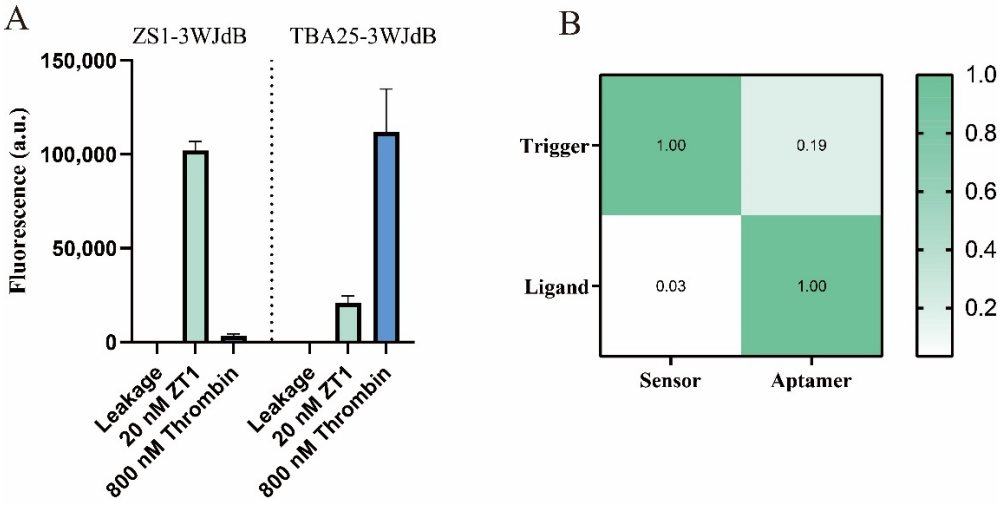

Figure 10. Aptamer-SWT orthogonality test. ZS1 and TBA25 were used as examples to investigate the orthogonality between the aptamer and SWT elements (SWT and aptamer template concentrations were both set at 10 nM, trigger template concentration at 20 nM, and ligand concentration at 800 nM). By comparing (**A**) the activated fluorescence peak values within 2 h across different groups and (**B**) the percentage calculated based on the activated fluorescence peak values (with the fluorescence value of the homologous group set to 1), it was observed that the aptamer and SWT elements exhibit good orthogonality. Error bars indicate the average value of three independent biological replicates ± s.d.

3.6.2. Heterologous Input OR Gate

Inspired by the previous exploration of the synergistic regulatory effects of the Aptamer-SWT system, the design concept for the heterologous input "OR" gate model involves placing the weaker regulatory aptamer upstream of the stronger regulatory SWT as a gating point, followed by the reporter gene 3WJdB. When the ligand molecule is introduced, the aptamer undergoes a conformational change upon specific binding with the ligand, which may disrupt the downstream SWT structure, making it more relaxed and allowing the expression of the downstream reporter gene, thereby producing a fluorescent signal. When Trigger RNA is introduced, it specifically binds to the Sensor RNA of

SWT, disrupting its stem-loop structure and weakening the termination effect at the gating point, thus enabling the downstream reporter gene expression and fluorescence output. When both the ligand and Trigger RNA are introduced simultaneously, the activation effect is even more pronounced (Figure 11A). However, due to the different mechanisms of action between the aptamer and SWT, their regulatory effects also exhibit certain differences. To achieve "OR" gate logic operation, we reduced the input concentration of Trigger RNA to weaken SWT activation and balance the regulatory effects of the two elements. Experimental results (with Trigger RNA template concentration set at 10 nM, ligand molecule thrombin concentration at 800 nM, and response module concentration at 10 nM) showed that ligand input alone resulted in a 2.08-fold increase in fluorescence activation, Trigger RNA input alone led to a 2.11-fold increase, and co-input of ligand and Trigger RNA yielded a 3.02-fold increase in fluorescence activation (Figure 11B). These results confirm the validity of the "OR" gate model.

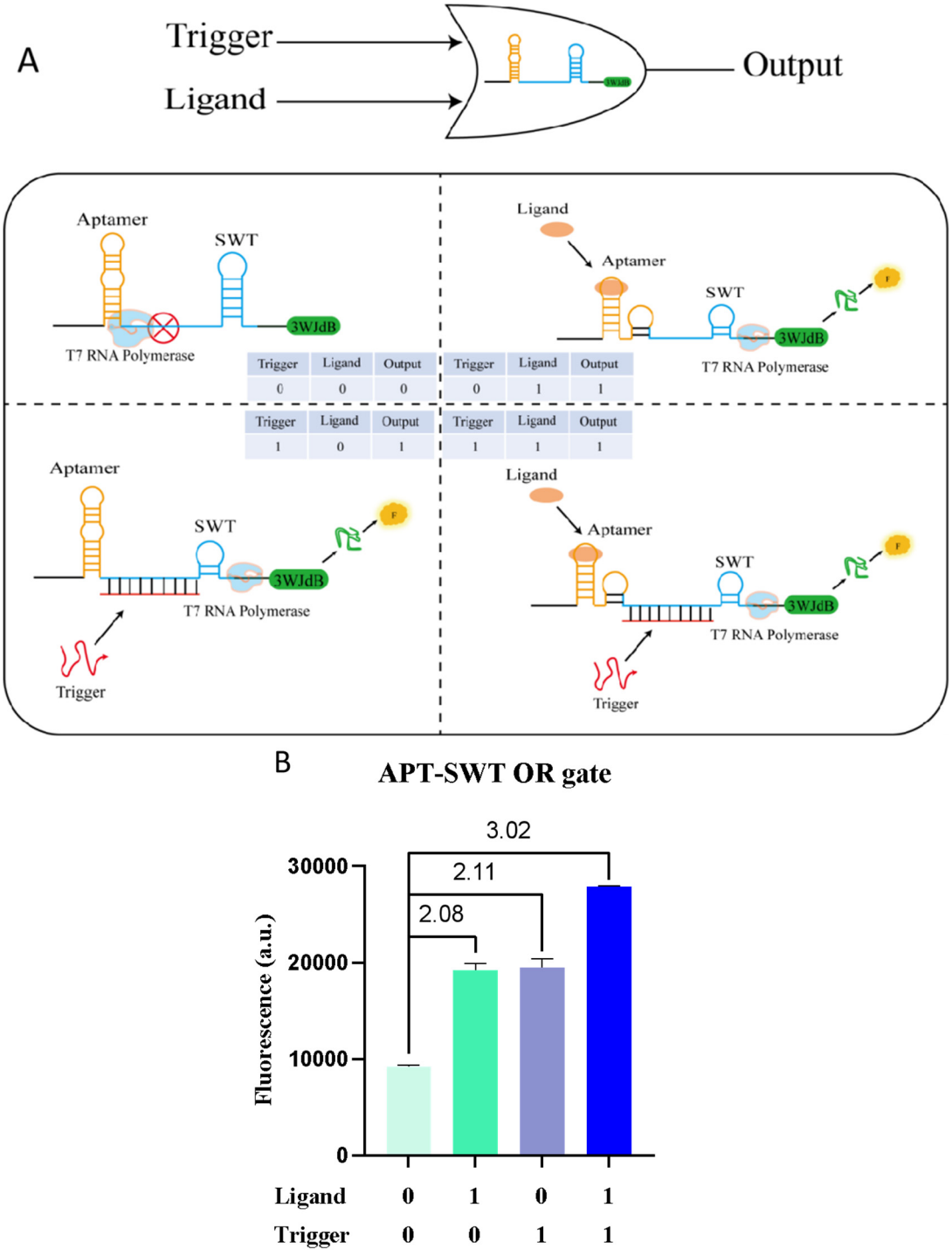

Figure 11. Construction and characterization of the aptamer-SWT heterologous input OR Gate. (**A**) Construction and mechanism: We combined the well-performing TBA25 and ZS1 aptamers, inserting TBA25 upstream of ZS1 to construct a heterologous input "OR" gate. When the ligand is introduced, the aptamer-ligand binding induces a conformational change, which may perturb the

structure of SWT, making it more relaxed and promoting transcription. When the trigger is introduced, the original stem-loop structure of SWT is disrupted, which also promotes transcription. (**B**) Performance characterization: The template concentration of trigger RNA is 10 nM, the ligand molecule thrombin concentration is 800 nM, and the response module concentration is 10 nM. Compared to the fluorescence signal output without any input, when only the ligand is introduced, there is a 2.08-fold increase in fluorescence activation; when only the trigger is introduced, there is a 2.11-fold increase; and when both the ligand and trigger are co-introduced, a 3.02-fold increase in fluorescence activation is observed. Error bars indicate the average value of three independent biological replicates ± s.d.

3.6.3. Heterologous Input AND Gate

The construction of the heterologous input AND gate is achieved by using the aptamer and SWT to regulate the correct folding of the reporter gene, enabling the correct output for the AND gate. Inspired by the design of the OR gate, we inserted an aptamer combined with a hairpin structure as the first gating point upstream of the reporter gene to hinder T7 RNAP elongation. The hairpin structure also further reduces leakage expression. The SWT is placed downstream of the reporter gene as the second gating point, interfering with the correct folding of the reporter gene. When only the ligand is input, the SWT interferes with the proper folding of the reporter gene, so no significant fluorescence activation occurs. When only trigger RNA is input, although the reporter gene can fold correctly, the hairpin structure after the aptamer also obstructs transcription, resulting in no substantial fluorescence activation. Only when both signals are co-input is a large fluorescence signal activation (Figure 12A). We first tested the regulatory potential of four aptamers for constructing the AND gate and found that the combination of TBA25 and ZS1 yielded results more in line with AND gate logic (Figure S11A). Additionally, when using 3WJdB as the reporter gene, SWT did not effectively interfere with its normal folding, possibly because 3WJdB consists of three Broccoli aptamers connected by a trivalent junction point, making it structurally complex and stable, not easily disrupted (Figure S11B). Therefore, when constructing the AND gate regulatory model with nucleic acid aptamers and SWT, we replaced 3WJdB with the structurally simpler Broccoli aptamer, whose proper folding is more easily interfered with. The results of the AND gate model testing (with Trigger RNA template concentration at 1 nM, ligand molecule thrombin concentration at 800 nM, and response module concentration at 10 nM) showed that when either the ligand or trigger RNA was input alone, there was no significant fluorescence output. However, when both signals were co-input, there was a 2.98-fold fluorescence activation (Figure 12B). These results confirm the validity of the heterologous input AND gate model.

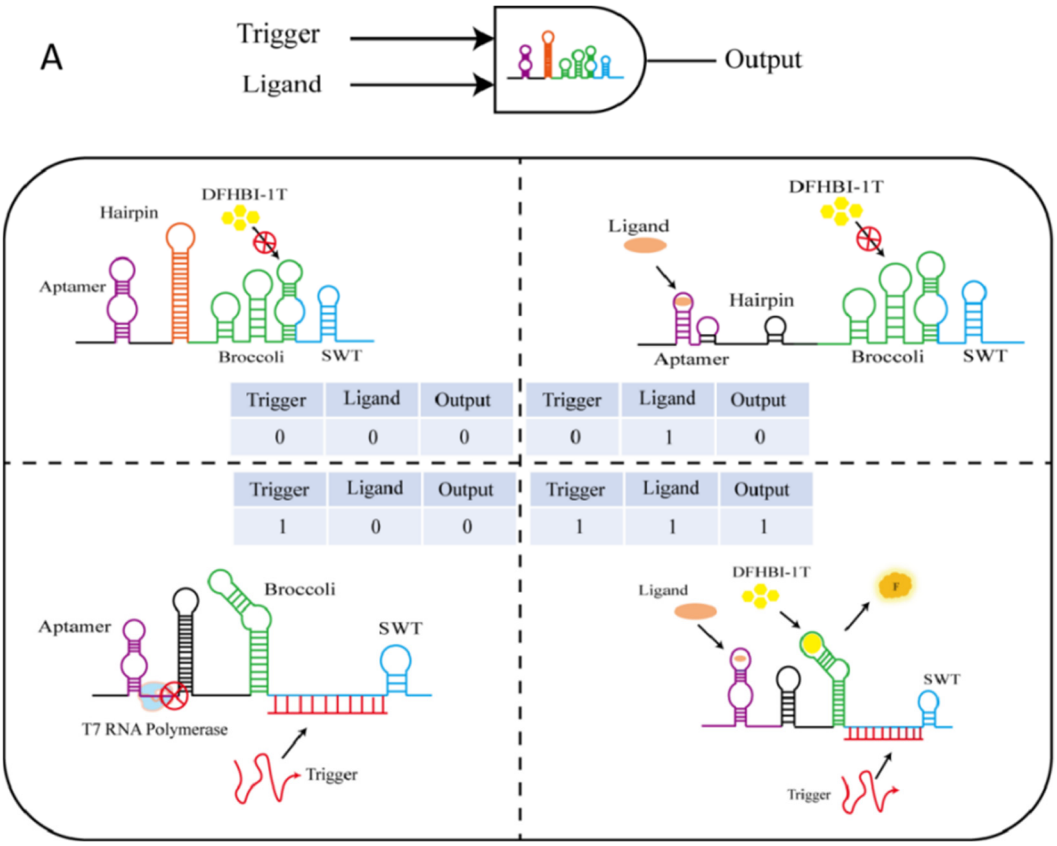

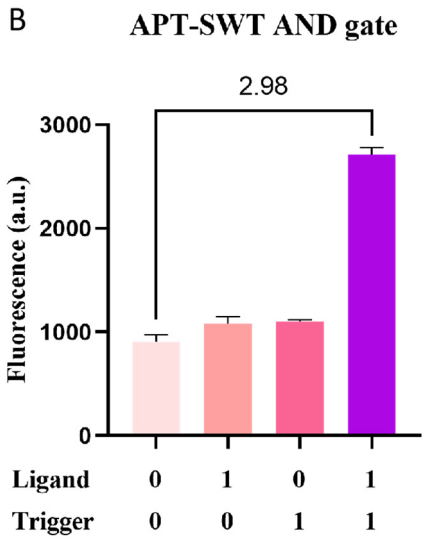

Figure 12. Construction and characterization of the aptamer-SWT heterologous input AND Gate. (**A**) Construction and mechanism: The construction of the heterologous input AND gate model is achieved by regulating the transcription process and the proper folding of the reporter gene. Here, we replaced 3WJdB with Broccoli. Inspired by the design of the heterologous input OR gate, we inserted TBA25 upstream of the reporter gene and added a hairpin structure to reduce leakage expression and hinder transcription, forming an aptamer-SWT OR gate. Additionally, SWT was introduced downstream of the reporter gene to interfere with the normal folding of Broccoli. When a trigger is input, despite interference with the structure upstream of the reporter gene, the downstream SWT still prevents the proper folding of Broccoli, resulting in no fluorescence activation. When a trigger is input, it binds to SWT, allowing Broccoli to fold normally, but the hairpin structure upstream of the reporter gene still hinders transcription. Only when both trigger and ligand are input simultaneously is fluorescence activation observed. (**B**) Performance characterization: The template concentration of trigger RNA is 1 nM, the ligand thrombin concentration is 800 nM, and the response module concentration is 10 nM. When both ligand and trigger are co-input, a 2.98-fold increase in fluorescence activation is observed. Error bars indicate the average value of three independent biological replicates ± s.d.

3.6.4. Construction of a Cascade Reaction Using Aptamer-SWT Integration

We used SWT to construct multi-layer cascade reactions and have already validated the orthogonality between aptamer and SWT. To extend the input sources for cascade reactions and respond to more complex environmental signals, this study combines aptamers with SWT to build a cascade reaction. We used thrombin as the input module (X), connected the well-performing TBA25 verified previously with the input signal ZT19 to form the signal conversion module (Y), and connected ZS19 with 3WJdB to form the output module (Z). When the ligand thrombin is introduced, TBA25 binds to thrombin, inducing a conformational change that promotes the expression of downstream genes, producing more ZT19 and ultimately generating more activated fluorescence signals (Figure 13A). We also explored the transcriptional regulatory effects of each module under different concentration conditions. Due to limitations in the transcription system, we fixed the output module concentration at 10 nM and investigated the changes in fluorescence activation peak values at input module concentrations of 0 nM, 50 nM, 200 nM, and 800 nM, and signal conversion module concentrations of 5 nM, 10 nM, and 20 nM. The results showed that when the ligand concentration of the input module was 800 nM, the promotion of the output fluorescence signal was significant. The best promotion occurred when the input ligand concentration was 800 nM, the conversion module concentration was 20 nM, and the output module concentration was 10 nM, greatly enhancing the final fluorescence output. This further validates the functionality of the cascade reaction and demonstrates that the aptamer can indeed be used for the transcriptional regulation of downstream genes (Figure 13B).

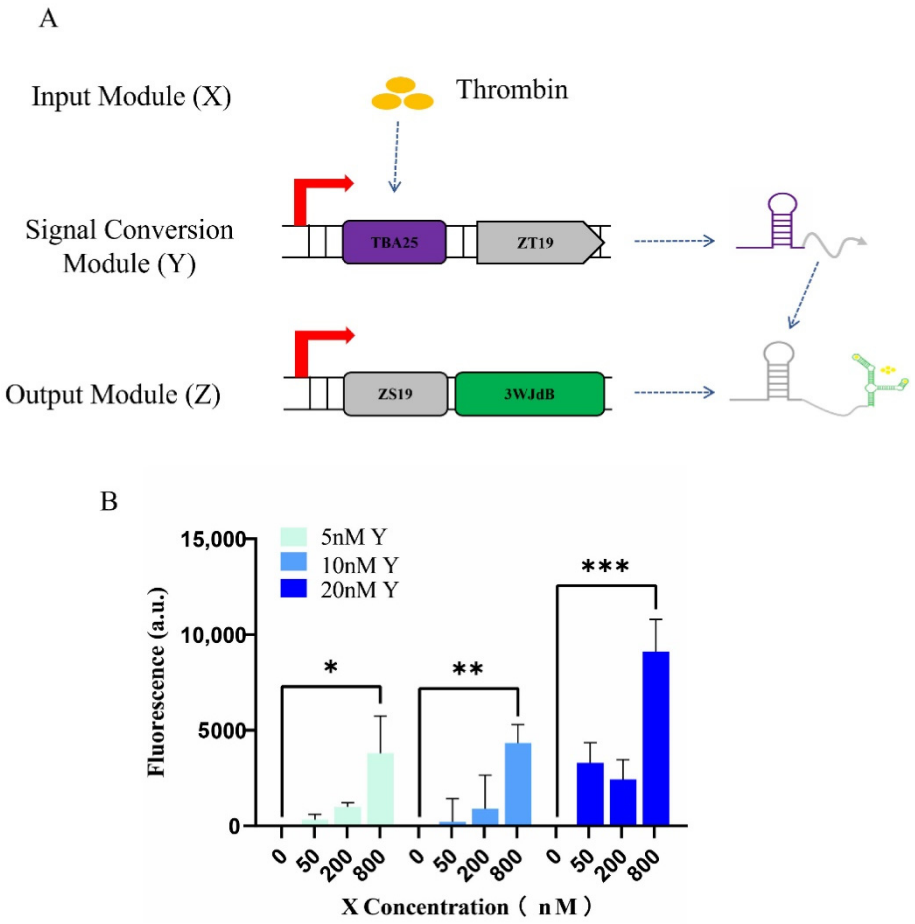

Figure 13. Construction and characterization of the aptamer-SWT cascade reaction. (**A**) Construction and mechanism: The entire cascade circuit is constructed with Ligand (Thrombin) as the input module (X), TBA25-ZT19 as the signal conversion module (Y), where TBA25 regulates the expression of ZT19; and ZS19-3WJdB as the output module (Z). (**B**) Performance characterization: The output module concentration was fixed at 10 nM (to better compare the regulatory effects of the input ligand and the conversion module, and to further validate the feasibility of the Aptamer-SWT combination), and the activation fluorescence peak values were investigated under conditions of input module concentrations of 0 nM, 50 nM, 200 nM, and 800 nM, and signal conversion module concentrations of 5 nM, 10 nM, and 20 nM. After inputting Ligand, significant fluorescence activation was observed, further demonstrating that nucleic acid aptamers can be used for transcriptional regulation of downstream genes. For data in (**B**), *t*-tests were performed on each construct; * $p < 0.05$, ** $p < 0.01$, and *** $p < 0.001$ indicate the fluorescence change is statistically significantly different. Error bars represent the standard deviation (s.d.) of three biological replicates.

4. Conclusions and Discussion

Gene expression regulation has always been a key focus in synthetic biology. Traditional gene expression regulation methods have gradually exposed many drawbacks and limitations, making the discovery of novel regulatory elements necessary. With the development of synthetic biology, an increasing number of novel gene elements have been designed and developed, which have improved the precision and flexibility of gene expression.

In previous studies, inspired by STARs, Hong et al. designed the switchable terminator (SWT) and combined it with the Toehold Switch for transcription and translation regulation. To precisely control the transcription process, we systematically explored the design strategies for switchable transcription terminators, developed and optimized an automatic design algorithm to improve the orthogonality of complex multi-layer circuits, and built a three-layer cascade circuit and an OR gate model *in vitro* based on SWT. In this study, on the one hand, we tested a series of SWT regulatory performances output by the algorithm, screening five SWT candidates with good performance, and further validated their reproducibility in regulating transcription in *E. coli*. Meanwhile, we constructed multi-layer cascade circuits *in vitro*, extending the cascade reaction to six layers, and also built four types of gene logic gate models, including AND, NOT, NAND, and NOR gates. On the other hand, we tested the transcriptional regulation effect of a novel regulatory element, the nucleic acid aptamer, and combined SWT with Aptamer to explore their synergistic effect on transcriptional regulation, constructing AND gate，OR gate，and cascaded circuit regulatory models with heterologous inputs. With the in-depth research on gene expression regulation in synthetic biology, the demand for gene elements

and circuits with low leakage expression and good orthogonality is increasing. Our research expands the methods and strategies in the field of gene expression regulation in synthetic biology and provides new elements for precise transcriptional regulation. Furthermore, in this study, both the SWT and aptamer-based regulatory mechanisms achieve transcriptional control through the introduction of exogenous input signals (nucleic acids or biochemical molecules). In principle, they can be tested in more complex biological systems; however, practical application in such systems still faces considerable challenges. First, the transcriptional machinery in complex biological systems differs significantly from that in prokaryotic systems. For instance, eukaryotes possess multiple RNA polymerases (such as RNA polymerases I, II, and III, which are responsible for synthesizing different types of RNA, including rRNA, mRNA, and tRNA, respectively, with rRNA accounting for the vast majority of cellular RNA), whereas prokaryotes typically have a single core multi-subunit RNA polymerase that recognizes different promoters through variations in the σ factor. Furthermore, transcription initiation in eukaryotic cells often requires various transcription factors or specific genomic contexts. Therefore, if these elements are to be applied in more complex organisms, they may require further modification or redesign to accommodate the characteristics of eukaryotic transcription. Second, the cellular environment in complex systems is more intricate, which increases the likelihood of RNA elements undergoing mutation, splicing, or degradation. This necessitates the development of highly stable RNA components. Additionally, the effective delivery of DNA templates or synthetic RNAs into complex organisms, particularly multicellular organisms, remains a challenge and may require the use of viral vectors, electroporation, or nanoparticle-based delivery systems. Despite these challenges, the aptamer-SWT regulatory system offers strong potential for broader application beyond *in vitro* or prokaryotic systems due to its modular and extensible design. This modularity allows for flexible customization in response to different input molecules and desired outputs, thereby enabling potential adaptability across diverse cellular environments.

DNA or RNA elements, due to their advantages such as low cellular burden, good biocompatibility, and rapid response, have a broad application prospect. They can be used for the construction of gene circuits or biosensors, nucleic acid therapy, drug detection, and other research fields. Li et al. developed the DREAM platform, which can design idealized cis-regulatory gene elements from scratch for gene expression regulation [53]; Ardjan J et al. used Toehold switches to build weighted computation circuits based on cell-free transcription and translation systems (TX-TL), and by introducing the σ^{28} factor and its inhibitor (anti-σ^{28}, with an N-terminal 10 × His tag and a C-terminal Myc tag), achieved biological "binary classification". This system can directly combine the classification of biomarkers with the generation of treatment methods, providing immediate personalized treatment for patients with different conditions [54]. Hong et al. developed a de novo designed single nucleotide-specific programmable ribosome regulator (SNIPR), which only binds and activates expression with the perfectly matched target sequence. A single nucleotide mutation in the target RNA results in significant thermodynamic loss, which can detect and locate gene mutations, making it a molecular probe for detecting and treating carcinogenesis [55]; Canoura, Yu et al. built biosensors based on Aptamers to detect fentanyl and tetrahydrocannabinol [56,57], providing new detection tools for public safety, healthcare, and forensic identification. Similarly, by exploring the regulatory effects of SWT and aptamer, we innovatively combined these two gene elements with different mechanisms of action, with the potential to integrate sensing and regulation. These could be used in gene therapy, metabolic pathway regulation, disease or drug biomarker detection, and other fields. Moreover, with the iterative development of AI algorithms, the Nicolaas team successfully predicted the performance of Toehold Switches using deep neural networks (DNN) [58], promoting the rational design and optimization of RNA elements. In the future, we can also combine experimental results with AI algorithms, further optimizing the design algorithm to output SWT or Aptamer with better regulatory performance, thus avoiding the complex screening, testing, and re-screening process, saving a lot of experimental costs and effort.

In summary, the strategy of combining nucleic acid aptamers with switchable transcription terminators to synergistically regulate downstream gene transcription is feasible. Although the actual regulatory performance and mechanisms differ, their combination enables multi-regulation within the same transcription system, improving transcriptional regulation's precision, flexibility, and programmability. This lays a theoretical foundation for solving societal, economic, and human health challenges.

Supplementary Materials

The following supporting information can be found at: https://www.sciepublish.com/article/pii/550, Table S1: DNA sequences for the transcriptional regulation system ; Figure S1: Plasmid map of pSG81; Figure S2: Plasmid map of pSG22; Figure S3: Secondary structure predictions of 21 SWT variants generated by the algorithm; Figure S4:

Fluorescence values of SWT under different states; Figure S5: Orthogonality prediction of candidate SWT; Figure S6: Six-layer cascade characterization; Figure S7: Characterization of the NAND gate using one-pot method; Figure S8: Candidate aptamer Mfold secondary structure prediction and AlphaFold 3 interaction structure prediction; Figure S9: Circular dichroism (CD) characterization of aptamers; Figure S10: The effect of the ligand thrombin on *in vitro* transcription; Figure S11: Investigation of APT-SWT heterogeneous input AND Gate construction.

Acknowledgments

We would like to thank Jongmin Kim of Pohang University of Science and Technology and Jianmin Yang, Yunquan Zheng, Feng Li, Mingmao Chen, and Li Chen of Fuzhou University for helpful discussion and suggestions.

Author Contributions

J.J. and S.G. conceived and designed the study. J.J., M.S. and S.Z. performed cloning and *in vitro* assay. J.J. designed multilayered circuits. J.J. wrote the original manuscript. S.G. and X.S. revised and edited the manuscript. All authors have given approval to the final version of the manuscript.

Ethics Statement

Not applicable.

Informed Consent Statement

Not applicable.

Funding

This work was supported by the Guiding Project of Fujian Provincial Department of Science and Technology (Grant No. 2023Y0006); Special project of Fujian Provincial Department of Finance (202309).

Declaration of Competing Interest

The authors declare that they have no competing interests.

References

1. Pope SD, Medzhitov R. Emerging Principles of Gene Expression Programs and Their Regulation. *Mol. Cell* **2018**, *71*, 389–397.
2. Mendillo ML, Santagata S, Koeva M, Bell GW, Hu R, Tamimi RM, et al. HSF1 drives a transcriptional program distinct from heat shock to support highly malignant human cancers. *Cell* **2012**, *150*, 549–562.
3. Gao X, Fu Y, Sun S, Gu T, Li Y, Sun T, et al. Cryptococcal Hsf3 controls intramitochondrial ROS homeostasis by regulating the respiratory process. *Nat. Commun.* **2022**, *13*, 5407.
4. Lamrabet O, Plumbridge J, Martin M, Lenski RE, Schneider D, Hindre T. Plasticity of Promoter-Core Sequences Allows Bacteria to Compensate for the Loss of a Key Global Regulatory Gene. *Mol. Biol. Evol.* **2019**, *36*, 1121–1133.
5. Dong C, Fontana J, Patel A, Carothers JM, Zalatan JG. Synthetic CRISPR-Cas gene activators for transcriptional reprogramming in bacteria. *Nat. Commun.* **2018**, *9*, 2489.
6. Wang T, Simmel FC. Riboswitch-inspired toehold riboregulators for gene regulation in *Escherichia coli. Nucleic Acids Res.* **2022**, *50*, 4784–4798.
7. Berens C, Groher F, Suess B. RNA aptamers as genetic control devices: The potential of riboswitches as synthetic elements for regulating gene expression. *Biotechnol. J.* **2015**, *10*, 246–257.
8. Hong S, Kim J, Kim J. Multilevel Gene Regulation Using Switchable Transcription Terminator and Toehold Switch in Escherichia coli. *Appl. Sci.* **2021**, *11*, 4532.
9. Zhao M, Kim J, Jiao J, Lim Y, Shi X, Guo S, et al. Construction of multilayered gene circuits using de-novo-designed synthetic transcriptional regulators in cell-free systems. *J. Biol. Eng.* **2024**, *18*, 64.
10. Chappell J, Takahashi MK, Lucks JB. Creating small transcription activating RNAs. *Nat. Chem. Biol.* **2015**, *11*, 214–220.
11. Wachsmuth M, Findeiss S, Weissheimer N, Stadler PF, Morl M. De novo design of a synthetic riboswitch that regulates transcription termination. *Nucleic Acids Res.* **2012**, *41*, 2541–2551.
12. Brophy JA, Voigt CA. Principles of genetic circuit design. *Nat. Methods* **2014**, *11*, 508–520.

13. Ceroni F, Boo A, Furini S, Gorochowski TE, Borkowski O, Ladak YN, et al. Burden-driven feedback control of gene expression. *Nat. Methods* **2018**, *15*, 387–393.
14. Salvail H, Breaker RR. Riboswitches. *Curr. Biol.* **2023**, *33*, R343–R348.
15. Wachsmuth M, Domin G, Lorenz R, Serfling R, Findeiss S, Stadler PF, et al. Design criteria for synthetic riboswitches acting on transcription. *RNA Biol.* **2015**, *12*, 221–231.
16. Green AA, Silver PA, Collins JJ, Yin P. Toehold switches: De-novo-designed regulators of gene expression. *Cell* **2014**, *159*, 925–939.
17. Neupert J, Karcher D, Bock R. Design of simple synthetic RNA thermometers for temperature-controlled gene expression in Escherichia coli. *Nucleic Acids Res.* **2008**, *36*, e124.
18. Stevens JT, Carothers JM. Designing RNA-based genetic control systems for efficient production from engineered metabolic pathways. *ACS Synth. Biol.* **2015**, *4*, 107–115.
19. Davidson EA, Ellington AD. Synthetic RNA circuits. *Nat. Chem. Biol.* **2007**, *3*, 23–28.
20. Mutalik VK, Qi L, Guimaraes JC, Lucks JB, Arkin AP. Rationally designed families of orthogonal RNA regulators of translation. *Nat. Chem. Biol.* **2012**, *8*, 447–454.
21. Groher F, Bofill-Bosch C, Schneider C, Braun J, Jager S, Geissler K, et al. Riboswitching with ciprofloxacin-development and characterization of a novel RNA regulator. *Nucleic Acids Res.* **2018**, *46*, 2121–2132.
22. Felletti M, Stifel J, Wurmthaler LA, Geiger S, Hartig JS. Twister ribozymes as highly versatile expression platforms for artificial riboswitches. *Nat. Commun.* **2016**, *7*, 12834.
23. Wurmthaler LA, Sack M, Gense K, Hartig JS, Gamerdinger M. A tetracycline-dependent ribozyme switch allows conditional induction of gene expression in Caenorhabditis elegans. *Nat. Commun.* **2019**, *10*, 491.
24. Larson MH, Greenleaf WJ, Landick R, Block SM. Applied Force Reveals Mechanistic and Energetic Details of Transcription Termination. *Cell* **2008**, *132*, 971–982.
25. Shin J, Noireaux V. Efficient cell-free expression with the endogenous *E. coli* RNA polymerase and sigma factor 70. *J. Biol. Eng.* **2010**, *4*, 8.
26. Alam KK, Tawiah KD, Lichte MF, Porciani D, Burke DH. A Fluorescent Split Aptamer for Visualizing RNA–RNA Assembly *In Vivo*. *ACS Synth. Biol.* **2017**, *6*, 1710–1721.
27. Reif R, Haque F, Guo P. Fluorogenic RNA nanoparticles for monitoring RNA folding and degradation in real time in living cells. *Nucleic Acid. Ther.* **2012**, *22*, 428–437.
28. Haque F, Shu D, Shu Y, Shlyakhtenko LS, Rychahou PG, Evers BM, et al. Ultrastable synergistic tetravalent RNA nanoparticles for targeting to cancers. *Nano Today* **2012**, *7*, 245–257.
29. Shu D, Khisamutdinov EF, Zhang L, Guo P. Programmable folding of fusion RNA *in vivo* and *in vitro* driven by pRNA 3WJ motif of phi29 DNA packaging motor. *Nucleic Acids Res.* **2014**, *42*, e10.
30. Filonov GS, Moon JD, Svensen N, Jaffrey SR. Broccoli: Rapid Selection of an RNA Mimic of Green Fluorescent Protein by Fluorescence-Based Selection and Directed Evolution. *J. Am. Chem. Soc.* **2014**, *136*, 16299–16308.
31. Bhadra S, Ellington AD. Design and application of cotranscriptional non-enzymatic RNA circuits and signal trans ducers. *Nucleic Acids Res.* **2014**, *42*, e58.
32. Akter F, Yokobayashi Y. RNA signal amplifier circuit with integrated fluorescence output. *ACS Synth. Biol.* **2015**, *4*, 655–658.
33. Hofer K, Langejurgen LV, Jaschke A. Universal aptamer-based real-time monitoring of enzymatic RNA synthesis. *J. Am. Chem. Soc.* **2013**, *135*, 13692–13694.
34. Pothoulakis G, Ceroni F, Reeve B, Ellis T. The spinach RNA aptamer as a characterization tool for synthetic biology. *ACS Synth. Biol.* **2014**, *3*, 182–187.
35. Kocalar S, Miller BM, Huang A, Gleason E, Martin K, Foley K, et al. Validation of Cell-Free Protein Synthesis Aboard the International Space Station. *ACS Synth. Biol.* **2024**, *13*, 942–950.
36. Huizenga DE, Szostak JW. A DNA aptamer that binds adenosine and ATP. *Biochemistry* **1995**, *34*, 656–665.
37. Hermann T, Patel DJ. Adaptive recognition by nucleic acid aptamers. *Science* **2000**, *287*, 820–825.
38. Daniels DA, Chen H, Hicke BJ, Swiderek KM, Gold L. A tenascin-C aptamer identified by tumor cell SELEX: Systematic evolution of ligands by exponential enrichment. *Proc. Natl. Acad. Sci. USA* **2003**, *100*, 15416–15421.
39. Parekh P, Tang Z, Turner PC, Moyer RW, Tan W. Aptamers recognizing glycosylated hemagglutinin expressed on the surface of vaccinia virus-infected cells. *Anal. Chem.* **2010**, *82*, 8642–8649.
40. Keefe AD, Pai S, Ellington A. Aptamers as therapeutics. *Nat. Rev. Drug Discov.* **2010**, *9*, 537–550.
41. Guo KT, Schafer R, Paul A, Gerber A, Ziemer G, Wendel HP. A new technique for the isolation and surface immobilization of mesenchymal stem cells from whole bone marrow using high-specific DNA aptamers. *Stem Cells* **2006**, *24*, 2220–2231.
42. Shangguan D, Li Y, Tang Z, Cao ZC, Chen HW, Mallikaratchy P, et al. Aptamers evolved from live cells as effective molecular probes for cancer study. *Proc. Natl. Acad. Sci. USA* **2006**, *103*, 11838–11843.
43. Ellington AD, Szostak JW. *In vitro* selection of RNA molecules that bind specific ligands. *Nature* **1990**, *346*, 818–822.

44. Tuerk C, Gold L. Systematic evolution of ligands by exponential enrichment: RNA ligands to bacteriophage T4 DNA polymerase. *Science* **1990**, *249*, 505–510.
45. Guo S, Xu Z, Lin L, Guo Y, Li J, Lu C, et al. Using CIVT-SELEX to Select Aptamers as Genetic Parts to Regulate Gene Circuits in a Cell-Free System. *Int. J. Mol. Sci.* **2023**, *24*, 2833.
46. Lee H, Xie T, Kang B, Yu X, Schaffter SW, Schulman R. Plug-and-play protein biosensors using aptamer-regulated *in vitro* transcription. *Nat. Commun.* **2024**, *15*, 7973.
47. Fornace ME, Huang J, Newman CT, Porubsky NJ, Pierce MB, Pierce NA. NUPACK: Analysis and Design of Nucleic Acid Structures, Devices, and Systems. 2022. Available online: https://chemrxiv.org/engage/chemrxiv/article-details/636c7089b588507d0045f283 (accessed on 1 September 2023).
48. Abramson J, Adler J, Dunger J, Evans R, Green T, Pritzel A, et al. Accurate structure prediction of biomolecular interactions with AlphaFold3. *Nature* **2024**, *630*, 493–500.
49. Yeung E, Dy AJ, Martin KB, Ng AH, Del Vecchio D, Beck JL, et al. Biophysical Constraints Arising from Compositional Context in Synthetic Gene Networks. *Cell Syst.* **2017**, *5*, 11–24 e12.
50. Avino A, Fabrega C, Tintore M, Eritja R. Thrombin binding aptamer, more than a simple aptamer: chemically modified derivatives and biomedical applications. *Curr. Pharm. Des.* **2012**, *18*, 2036–2047.
51. Iyer S, Doktycz MJ. Thrombin-Mediated Transcriptional Regulation Using DNA Aptamers in DNA-Based Cell-Free Protein Synthesis. *ACS Synth. Biol.* **2013**, *3*, 340–346
52. Wang J, Yang L, Cui X, Zhang Z, Dong L, Guan N. A DNA Bubble-Mediated Gene Regulation System Based on Thrombin-Bound DNA Aptamers. *ACS Synth. Biol.* **2017**, *6*, 758–765.
53. Li Z, Zhang Y, Peng B, Qin S, Zhang Q, Chen Y, et al. A novel interpretable deep learning-based computational framework designed synthetic enhancers with broad cross-species activity. *Nucleic Acids Res.* **2024**, *52*, 13447–13468.
54. Van Der Linden AJ, Pieters PA, Bartelds MW, Nathalia BL, Yin P, Huck WTS, et al. DNA Input Classification by a Riboregulator-Based Cell-Free Perceptron. *ACS Synth. Biol.* **2022**, *11*, 1510–1520.
55. Hong F, Ma D, Wu K, Mina LA, Luiten RC, Liu Y, et al. Precise and Programmable Detection of Mutations Using Ultraspecific Riboregulators. *Cell* **2020**, *180*, 1018–1032 e16.
56. Canoura J, Liu Y, Perry J, Willis C, Xiao Y. Suite of Aptamer-Based Sensors for the Detection of Fentanyl and Its Analogues. *ACS Sens.* **2023**, *8*, 1901–1911.
57. Xie Y, She JP, Zheng JX, Salminen K, Sun JJ. Rapid nanomolar detection of Delta (9)-tetrahydrocannabinol in biofluids via electrochemical aptamer-based biosensor. *Anal. Chim. Acta* **2024**, *1295*, 342304.
58. Angenent-Mari NM, Garruss AS, Soenksen LR, Church G, Collins JJ. A deep learning approach to programmable RNA switches. *Nat. Commun.* **2020**, *11*, 5057.